# Tiered approach for rapid damage characterisation of infrastructure enabled by remote sensing and deep learning technologies

Nadiia Kopiika<sup>(a)</sup>, Andreas Karavias<sup>(b)</sup>, Pavlos Krassakis<sup>(b)</sup>, Zehao Ye<sup>(a)</sup>, Jelena Ninic<sup>(a)</sup>, Nataliya Shakhovska<sup>(e,c,d)</sup>, Nikolaos Koukouzas<sup>(b)</sup>, Sotirios Argyroudis<sup>(e,f)</sup>, Stergios-Aristoteles Mitoulis<sup>(a,f)</sup>

- (a) University of Birmingham, Edgbaston, Birmingham, B15 2TT, UK
- (b) Centre for Research and Technology Hellas (CERTH), 15125 Athens, Greece
- (c) Lviv National Polytechnic University, Stepana Bandery St, 12, L'viv, Lvivska oblast, 79000, Ukraine
- (d) University of Agriculture in Krakow, Podłużna 3, 30-239, Poland
- (e) Brunel University London, Kingston Lane, Uxbridge Middlesex, UB8 3PH, UK
- (f) MetaInfrastructure.org, London, UK

Corresponding author:

Stergios-Aristoteles Mitoulis, S.A.Mitoulis@bham.ac.uk

#### 1 Abstract

Critical infrastructure such as bridges are systematically targeted during wars and conflicts. This is because critical infrastructure is vital for enabling connectivity and transportation of people and goods, and hence, underpinning the national and international defence planning and economic growth. Mass destruction of bridges, along with minimal or no accessibility to these assets during natural and anthropogenic disasters, prevents us from delivering rapid recovery. As a result, systemic resilience is drastically reduced. A solution to this challenge is to use technology for stand-off observations. Yet, no method exists to characterise damage at different scales, i.e. regional, asset, and structural (component), and more so there is little or no systematic correlation between assessments at scale. We propose an integrated three-level tiered approach to fill this capability gap, and we demonstrate the methods for damage characterisation enabled by fit-for-purpose digital technologies. Next, this method is applied and validated to a case study in Ukraine that includes 17 bridges. From macro to micro, we deploy technology at scale, from Sentinel-1 SAR images, crowdsourced information, and high-resolution images to deep learning for damaged infrastructure. For the first time, the interferometric coherence difference and semantic segmentation of images were deployed to improve the reliability of damage characterisations from regional to infrastructure component level, when enhanced assessment accuracy is required. This integrated method improves the speed of decision-making, and thus, enhances resilience.

**Keywords**: critical infrastructure, damage characterisation, targeted attacks, restoration

#### 2 Introduction

Critical infrastructure assets, such as bridges, have a vital role in countries' accessibility, mobility and hence economies. They enable the smooth flow of people, vehicles, and goods across various obstacles like water bodies, canyons, and valleys. Therefore, systematic maintenance and monitoring of their service level is of paramount importance to ensure their undisrupted operation [1]. During targeted attacks, which are frequent during wars and conflicts, bridges are targeted due to their crucial role. The presence of violence and hazardous conditions in conflict zones hinders conventional approaches to damage assessment, including manual detection and on-site surveys conducted during hostilities. In the event of mass destruction of critical infrastructure entities followed by limited accessibility, our ability to enhance resilience through rapid assessments and restoration is hindered [2], leading to

significant direct and indirect losses, and hence, delays in restoring normal economic activity [3]. Therefore, an integrated assessment framework leveraged by digital technologies is needed, combining assessments at different scales, i.e. regional, infrastructure asset, and component, to facilitate restoration strategies and provide intelligence to recovery mechanisms, for decision-makers, governments, and funders to prioritise investments. The research is driven by the conviction that gaining a deeper insight into the immediate and long-term impacts of transport infrastructure disruption is crucial for shaping effective policies, promoting global cooperation, and ultimately, striving to rebuild urban environments devastated by conflict.

# 2.1 Stand-off observations for damage characterisation

Critical asset safety is normally assessed by on-site inspections and testing [4],[5], to inform decisions for targeted maintenance and restoration. These procedures are typically time-consuming and costly [6]. They are biased as they heavily rely on engineering judgment, and inaccurate due to the uncertainty imposed by ageing and climate change. Inspections are in some cases impossible, due to safety risks and inaccessibility. Extensive damage often requires spatial large-scale inspections, nevertheless, these may slow down the recovery process because they rarely account for the importance and interdependencies of assets at the regional level. This inadequacy renders them insufficient for the effective post-disaster management of large portfolios of assets and regions [7],[8]. Therefore, there is an urgent need for more reliable and rapid decision-making for prioritisation of restoration strategies that will use disparate inspection, testing and other digital data available after natural hazards, such as floods [9], earthquakes [10], landslides [11], and conflicts [12] to accelerate recovery[13]. Available methods include e.g., Global Position System (GPS), terrestrial Synthetic Aperture Radar (SAR) Interferometry (InSAR), and digital image correlation (DIC) [13],[14],[15],[16]. However, these methods are either effective at the macroscale, facilitating recovery at the regional scale, or at the microscale, e.g., UAVs, GNSS [17],[18], where data can be used to develop informational models, e.g. BIM [19]. In recent times, the analysis of satellite imagery has become a prospective tool for remote evaluation of infrastructure damage. The advancement of deep learning has endowed existing methods with distinct capabilities for identifying destruction by automatically detecting changes in satellite images from pre-war to wartime. Yet, these technologies have not been integrated to make decisions on different scales. In regard to bridges, stand-off damage characterisation is so far mainly focused on measuring structural deflections [20],[21], soil settlements [22], cracking [23],[24] and corrosion [25] as indicators of damage based on monitoring and mapping. Structural health monitoring at regional, asset and component levels with the use of computer vision-based [26] and remote technologies facilitate the assessment, management, and maintenance of bridges [26], [27]. This way, efficient decision-making toward restoration measures and infrastructure recovery is underpinned both at macro and micro scale.

#### 2.2 Use of InSAR imagery and open data in infrastructure assessment

Earth Observation (EO) technologies are applied for non-invasive observation and evaluation of affected areas using satellite images and geospatial approaches. In recent years, EO and especially Synthetic-Aperture Radar (SAR) images are increasingly being used as a tool for rapid mapping and damage characterisation after disasters, such as earthquakes and floods [29],[30],[31],[32]. Combination of Geospatial Intelligence (GEOINT) [33],[34], and EO products of geospatial data also facilitates the identification of spatial patterns related to hazard susceptibilities that may lead to infrastructure vulnerabilities [35],[36],[37],[38]. Another example is the identification of earthquake-induced building damage using backscatter intensity and phase signals from Interferometric Synthetic-Aperture Radar (InSAR) images [39],[40],[41]. In doing so, the Coherent Change Detection (CCD) techniques can utilise the phase signal correlation of InSAR products by comparing land changes before and after the events, to detect the affected areas. This enables to a certain degree the characterisation of damage of infrastructure and natural environment [41],[42],[43]. Most of previous studies were primarily focused on assessing damages resulting from natural hazards, for which destructions in certain regions are associated with considerable geographical patterns and correlated features. However, structural destructions, caused by human-induced hazards (e.g. wars, terrorist attacks, etc) follow different trends; destroyed assets, thus, are sparsely

distributed in intricate urban environments, occupying only a minor part of urban areas, while the majority of the surrounding environment remains unaffected. Such cases are associated with a notable class imbalance because the number of undamaged buildings and structures significantly exceeds that of the affected ones. As a result, the combined effect of considerable class imbalance and the heterogeneous nature of urban environments cause significant challenges in identifying affected assets across the entire city/ region. Such an obstacle could be eliminated by the implementation of additional pre-investigation with the use of open access data (e.g. crowdsourcing, Open Street Maps, online open access platforms, etc). Another common feature of the majority of studies is their reliance on high-resolution satellite imagery. Inaccessibility of such high-resolution satellite data during both, the duration of the conflict and post-conflict rehabilitation triggers significant hurdle to damage assessment with this approach. This lack of availability has a considerable impact on the broader public, as well as causing challenges for research purposes, aiming to monitor urban warfare and build prioritization and rehabilitation strategies with this method. Given the following circumstances, the application of medium-resolution satellite imagery, especially in conditions of high level of class imbalance (heterogeneity of damage level), becomes compelling and noteworthy for the damage characterisation of infrastructure assets on conflict-torn territories.

### 2.3 Deep learning techniques in damage detection

Deep learning techniques have emerged as powerful tools in the field of damage detection, revolutionizing the approach towards the identification and assessment of structural impairments across various domains. Leveraging the capabilities of neural networks with multiple layers, these techniques excel in learning intricate patterns and representations from vast datasets, enabling highly accurate and efficient damage detection.

Deep learning (DL) is a subset of machine learning (ML) within artificial intelligence (AI), which is essentially a deep neural network with three or more layers. Computer Vision (CV) is another subset method of AI and is concerned with the automatic extraction of useful information from image data, facilitating assessment, understanding or representing the underlying physical world, either qualitatively or quantitatively [44]. The recent increase in computation power enhanced the usage of DL and CV for handling a variety of ML tasks in practical physical-world scenarios [45],[46],[47]. These technologies have been increasingly used in civil engineering to automatically perform a number of tasks related to inspections, monitoring, and assessment of infrastructure, such as 3D model reconstruction and damage detection. Automated vision-based structural inspection using semantic segmentation algorithms enables rapid analysis of the conditions of the transport infrastructure assets affected by hazards, in conditions of limited time, accessibility and resource constraints [48]. CV tasks enhanced by Deep Learning empower a machine to ingest image and text data, enabling it to autonomously discern and identify the fundamental characteristics of a damaged asset. This involves the utilization of advanced neural network architectures to automatically extract intricate patterns and relevant features from the provided data, facilitating a more nuanced and precise understanding of the condition and attributes of the impaired asset. The integration of DL in CV tasks significantly enhances the machine's ability to comprehend and interpret complex visual and textual information related to asset damage, contributing to more sophisticated and efficient automated analysis processes. This approach requires the following tasks as described in Figure 1, [49]: (a) image classification based on labelled image (e.g. spalling, crack); (b) patch-wise classification where each patch is classified as either presenting a crack or not; (c) object localisation where bounding box indicates the position of the defect; (d) object localisation a heatmap; (e) object detection; (f) semantic segmentation to classify individual pixels. Thus, CV algorithms, assist in localising and quantifying structural defects and damages [50],[51], eliminating the necessity for labour-intensive and highly subjective on-site inspections [52].

The transformer-based architecture method outlined in [53] has demonstrated notable efficacy and is progressively gaining widespread acceptance. method of transformer-based architecture has demonstrated impressive performance and is steadily becoming mainstream. Researchers have directed their attention not only towards the refinement of model architecture but also towards enhancing the quality and quantity of training data. Notably, training on large-scale datasets, in particular with large language models has showcased their robust zero-shot and few-shot generalization capabilities, as discussed in [54] and [55]. Noteworthy, a substantial part of damage

detection techniques relies on the neural network approach. The Bidirectional Feature Pyramid Network model, introduced in [56] has been instrumental in locating and segmenting damage, achieving a commendable detection accuracy of 96%. However, the segmentation accuracy quantified using the mean Intersection Over Union (IOU) metric stands at approximately 83%. These damages were characterized by their small size and occurred under diverse lighting conditions. The damages were small in size and in different lighting conditions. The utilization of a pre-trained YOLO (You Only Look Once) model has also been explored. Data augmentation techniques have been employed to increase the dataset, as well as transfer learning of trained models based on the ImageNet dataset [57]. Among the models considered, the one based on the Mask Region-based Convolutional Neural Network (R-CNN) architecture has demonstrated superior performance, achieving an accuracy rate of 64%. A comprehensive comparative analysis between Mask R CNN and Yolo is presented in [58]. The study takes into account diverse data types, encompassing visual images, point cloud, infrared thermal imaging, ground-penetrating radar, vibration response, and other relevant types of data. Moreover, the research involves a meticulous comparison between two-stage and one-stage methods. The findings of this research highlight that, for facilitating effective bridge damage detection, a synergistic approach employing remote sensing combined with intelligent algorithms is invaluable for expeditious inspections, particularly targeting high-risk components such as piers and abutments.

Therefore, deep learning techniques have significantly advanced the field of damage detection by providing robust and versatile tools for analysing diverse data sources. These techniques offer a promising avenue for improving the efficiency, accuracy, and automation of structural health monitoring across various domains.

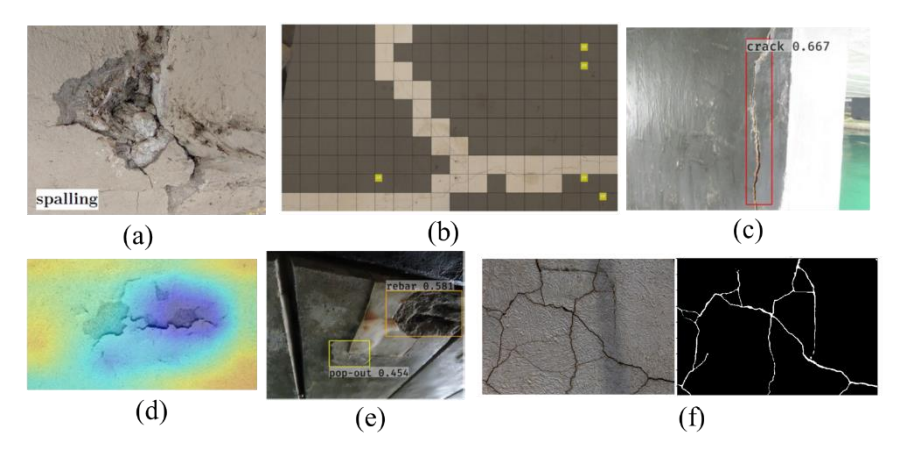


Figure 1 CV tasks empowered by DL for (a) image classification; (b) patch-wise classification; (c-d) object localisation; (e) object detection; (f) semantic segmentation.

#### 2.4 Main problem, knowledge gaps and novelty of this paper

Bridges, as vital components of transport infrastructure, play an important role for the economy and prosperity of societies. Extensive destruction of bridges, coupled with limited or no access to these critical assets during and on the aftermath of extensive natural or human-made disasters, hinders our ability to build resilience into critical infrastructure and communities. This is because damage assessment that includes the damage mode and cause, the extent, also known as damage level, the accessibility and its interdependencies with other assets and systems, and availability of resources (funds, labour, materials) are all dominant factors in decision making. These define adaptation and restoration strategies, and this paper deals with this challenge with a focus on damage characterisation.

Even though there has been vertical research in specific technologies for damage identification at (i) macro (regional) and (ii) micro (asset or component) level, there is no framework that integrates different scales of damage characterisation. Thus, vertical research has not been integrated into an unified engineering framework, while most of this vertical research was conducted in computer science and/or earth observation sciences, which neglects

engineering principles and practice. Therefore, research either misses the importance of asset damage state in (i), which may affect the operability of the region, or misses the state of the functionality level of the region in (ii) that may prevent the timely restoration of the assets. In both cases, resilience might be dramatically affected by this absence of integration of damage characterisation at different scales. This is a challenging and unique gap in the knowledge toward this paper is contributing.

In addition, the common approach, used for the assessment of natural hazards-induced damages with satellite imagery should not be directly used for human-induced hazards (e.g. wars, terrorist attacks, etc), which form a separate unique group. Infrastructure destruction during anthropogenic disasters is associated with high-class imbalance, occupying only a minor part of urban areas, surrounded by unaffected environment, in contrast to damages due to natural hazards, following geographical patterns. Consequently, the notable class imbalance and the diverse characteristics of urban environments cause certain challenges in the identification of affected assets within the whole infrastructural system. Moreover, the unavailability of high-resolution satellite data in conflict-prone regions due to security reasons additionally highlights the specific nature of human-induced hazards. Given the increased global risk of terrorist attacks, there is a pressing need for an integrated approach to quickly assess destruction during ongoing hostilities. This is crucial for strategic rehabilitation planning and prioritization in any country. This raises the obvious question: how can be performed damage characterization of infrastructural assets in the context of limited access to them, relying only on open-access informational sources?

To our best knowledge, this is the first tiered approach, integrating disparate open-access sources for multi scale for rapid damage characterisation of infrastructural assets, operated in conflict-prone regions. This paper puts forward a novel framework which is the first of its kind that aims to use disparate technologies and openly available data to characterise damage at different scales from regional, to asset, to component to ultimately offer rapid and well-informed decisions toward restoration and hence enhance resilience (see Figure 2). The focus is on regions and networks that include bridges, affected by shelling as a result of war and conflict. This framework is unique in that it identifies damage of critical infrastructure at the regional and asset level, using the InSAR Coherent Change Detection (CCD) method. The interferometric coherence difference values were used to characterise the damage level. This is valuable in case access to the region and assets is limited or not possible, thus severely delaying decision-making for restoration. CCD-based assessments were validated using additional stand-off observations, i.e. inspection records, open data, crowdsourcing, and available satellite images and photographs. When asset level CCD information is not adequate to make a decision regarding damage characterisation, another novel methodology is used. This employs the damage detection at the component level, using semantic segmentation for automatic localisation and damage classification. The method scouts a number of appropriate AI pre-trained big models for component-level damage detection in the context of post-disaster inspection, taking into consideration the uncertainties in the obstruction of the subject and complex backgrounds. This framework is demonstrated in a case study region in Ukraine, aimed at quickly characterising post-conflict damage in transport infrastructure at asset and component scale within a short time frame.

# 3 Methodology for damage assessment from regional to component level

#### 3.1 Methodology, framework and data for damage analysis at different levels

Figure 2 describes in detail the framework for damage characterisation that leads to decisions. The ultimate goal of the framework is to minimise the decision-making time using only openly available data and hence avoiding costly invasive methods, which in some cases are impossible due to e.g. inaccessibility. The figure also provides a nomenclature of the different levels of assessment, i.e. region (R), asset (A) and component (C) level. The methodology starts with the threat identification and proceeds with the selection of the level of assessment: for all assets openly available data are used to map critical assets and interdependencies. Damage detection at regional and asset level is conducted (see more detail in Figure 3), by employing remote sensing technologies, e.g. ESA open hub. If the damage characterisation can be conducted with a high level of confidence (and hence adequate damage

characterisation), then the only hurdle to design and apply a restoration strategy is the connectivity and hence accessibility to the asset. For example, if the asset is a bridge, connectivity to the bridge will be sought both through the road in which the bridge belongs to and through other routes that may lead to critical components, e.g. foundations. If access to the asset is possible, then we can proceed with decisions, designs and restoration strategy. If not, then we will have to assess the level of damage of the connection. In this case, damage characterisation for the connectivity (e.g. roads) is also conducted using remote sensing.

If damage characterisation is not adequate for the restoration, this means that more information is required to make a decision for the recovery measures. That takes us to a higher level of accuracy by characterising damage at component (C) level, using high-resolution images from open-access platforms (see Figure 4). Based on this we can then make a decision that the damage characterisation is adequate to proceed with the restoration strategy. Otherwise, better quality data should be sought (e.g. testing, inspections) to proceed with restoration.

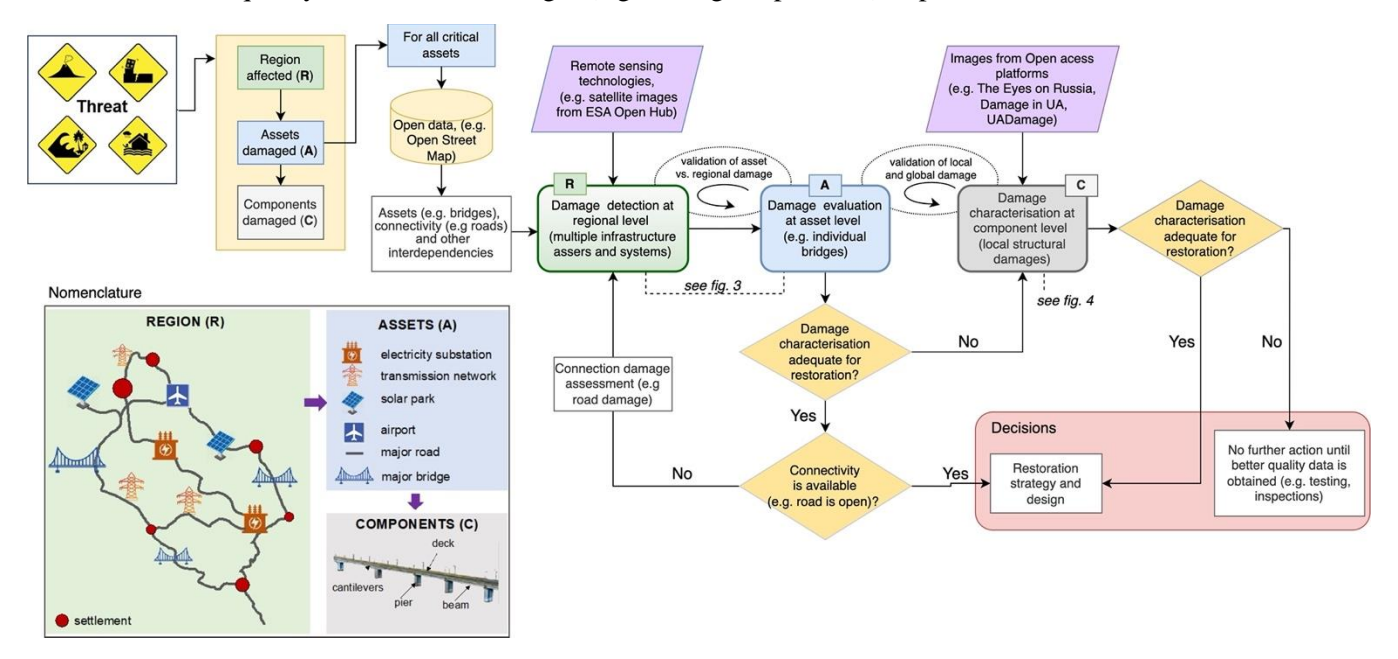


Figure 2. Framework for damage characterisation at regional(R), asset(A) and component(C) level toward decisions for restoration.

#### 3.2 Regional and asset level damage characterisation

Damage characterisation at regional and asset levels comprises utilization of the open-access Setinel-1 Single Look Complex (SLC) products and OpenStreetMap (OSM) data for the period of interest (time of extensive damage in the study area).

The processing method for damage characterisation at regional and asset level (*Figure 3*) is fourfold: (1) location and geometry data of critical assets, residing within the boundaries of the selected study area; (2) generation of the Coherence and Coherent Change Detection (CCD) products using Sentinel-1 SAR SLC images; (3) development of a semi-automated method for the detection of damage on infrastructure assets, e.g. bridges; and (4) damage evaluation at asset level using CCD values.

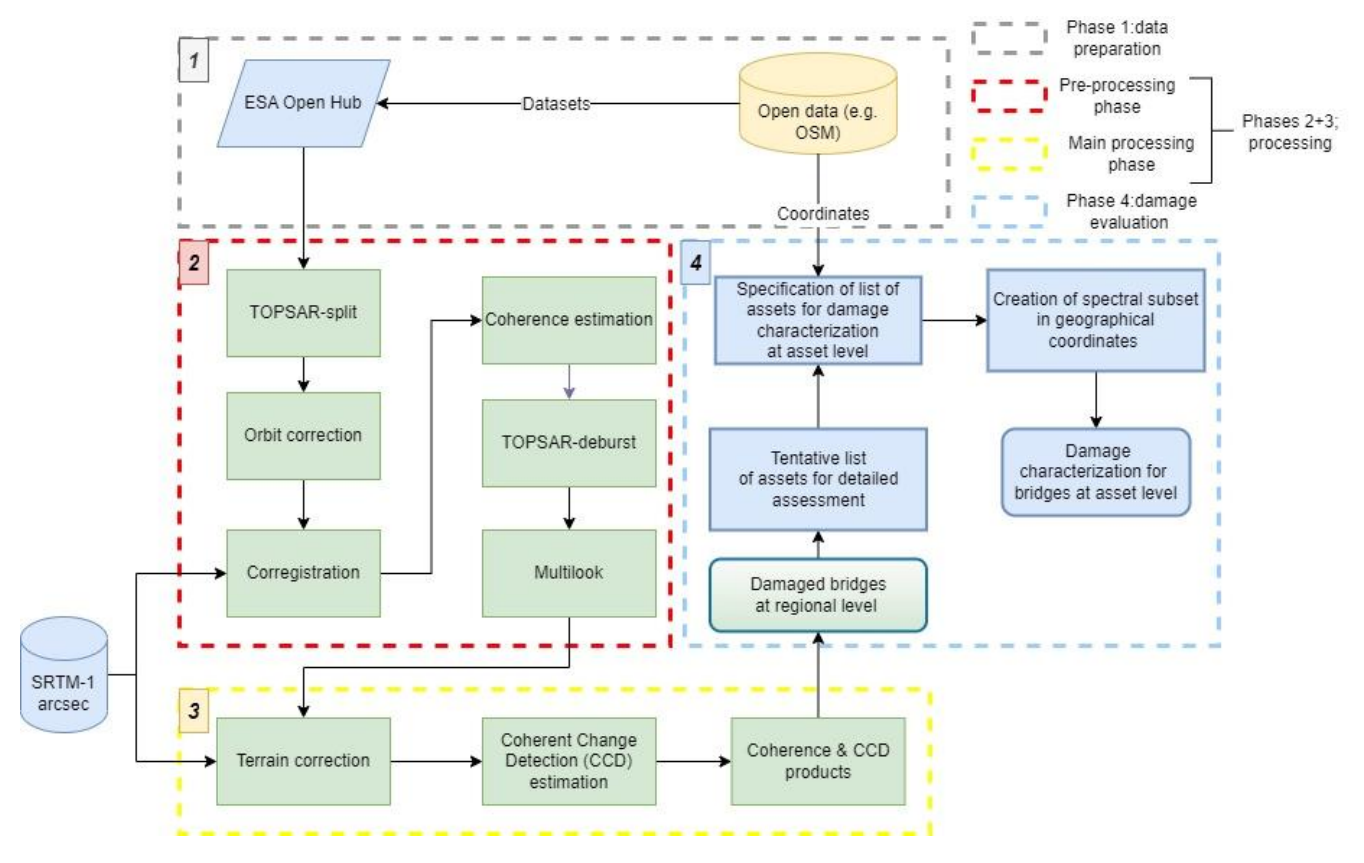


Figure 3 Workflow of the satellite and geospatial datasets that were implemented for the four-fold process. The four polygons indicate main phases of Sentinel-1 data preparation (1<sup>st</sup>, grey polygon); pre-processing (2<sup>nd</sup> red polygon); main processing (3<sup>d</sup>, yellow polygon); and damage evaluation (4<sup>th</sup>, blue polygon).

The **first phase** (1) of assessment includes obtaining Sentinel-1 mission interferometric wide swath (IW) SAR images in ascending and descending geometry, covering the area of the region and assumed time of hazard. The Sentinel-1 mission consists of two satellites, Sentinel-1A and Sentinel-1B, sharing the same orbital plane. This mission has a wide swath width (250 km) and revisit time of 12 days, since the December of 2021 due to the Copernicus Sentinel-1B anomaly related to the instrument electronics power, leaving it unable to deliver radar data [59]. The pixel spacing is 2.3 m in the slant range and 14.1 m in azimuth, which translates to 5 m in ground range and 20 meters in azimuth resolution for a single-look image [60]. Simultaneously, for preliminary estimation of the geographic coordinates of affected assets was used data from open access platforms, (e.g. OpenStreetMap (OSM) [61], crowdsourcing [62],[63],[64]), including transport route disruption, interrupted connectivity in the region, destruction of the asset, reported in media. OpenStreetMap (OSM) is a publicly accessible dataset providing geospatial data in global scale that are related with land uses, transportation networks, and infrastructures [61]. This dataset undergoes continuous updates from users worldwide, making it an important source of geospatial information for both commercial and research applications.

The **second phase** (2) includes the pre-processing and the main processing of Sentinal-1 SAR SLC images using the open software SNAP. The left part of the workflow describes the process of splitting the images on the selected sub-swath with the specific bursts that cover the study area (TOPSAR split) and orbital correction by using the precise orbit files (Orbit correction). Subsequently, the images were corregistrated using the Digital Elevation Model of Shuttle Radar Topography Mission (DEM SRTM) -1 arcsec [65] in order to generate interferometric pairs before and after the damage. Furthermore, a coherence estimation was implemented in every interferometric pair followed by the "TOPSAR-deburst" and "Multilook" steps. After completing this stage, the coherence products were geocoded using the DEM SRTM-1 arcsec and grouped in stacks in order to calculate the CCD.

Damage detection at the **third phase** (3) is based on the geospatial analysis for 2 stacks of images, containing two pre-damage products and pre- and post- damage products, respectively. InSAR coherence products, calculated for two pairs of SAR images, served as an indicator of the similarity in radar reflections between certain datasets. The result represents the level of correlation in the phase of the corresponding pixels of the two images. Any changes in the backscattered signal of the satellite are recognized as decorrelation of the phase. As a result, changes in the scene from one acquisition to the next are detected. Changes between the two images reduces the coherence value and negatively affects the accuracy over the distance measurement between the antenna of the satellite and the Earth's surface [66]. The coherence ( $\gamma$ ) which is also defined as the complex correlation coefficient between two SAR scenes  $u_1$  and  $u_2$ , is estimated using Eq. (1) below:

$$\gamma = \frac{E\left[u_1 u_2^*\right]}{\sqrt{E\left[\left|u_1\right|^2\right]} \sqrt{E\left[\left|u_2\right|^2\right]}} \tag{1}$$

where *E*{} represents the mathematical expectation and \* is the complex conjugate operator. The range of coherence values ranges from 0 (low coherence) to 1 (high coherence). Pixels with high coherence values are characterised as stable with very small variations over time, while low coherence values indicate high to very high changes, respectively. Coherence is utilised here to identify damage of the built environment [67],[43].

Regarding CCD, this requires three images by pairing two images ( $\rho$ ) acquired before the event (pre), and two images, one before and one after the event (post) [68]. The CCD is defined as per Eq. (2) below:

$$CCD = \rho(pre) - \rho(post) \tag{2}$$

CCD values range from -1 to 1. Positive values represent areas with significant differences, indicating land changes. Values close to zero indicate relatively stable areas between satellite passes, and negative values could be related to the appearance of new stable areas during the interval between the two coherence products.

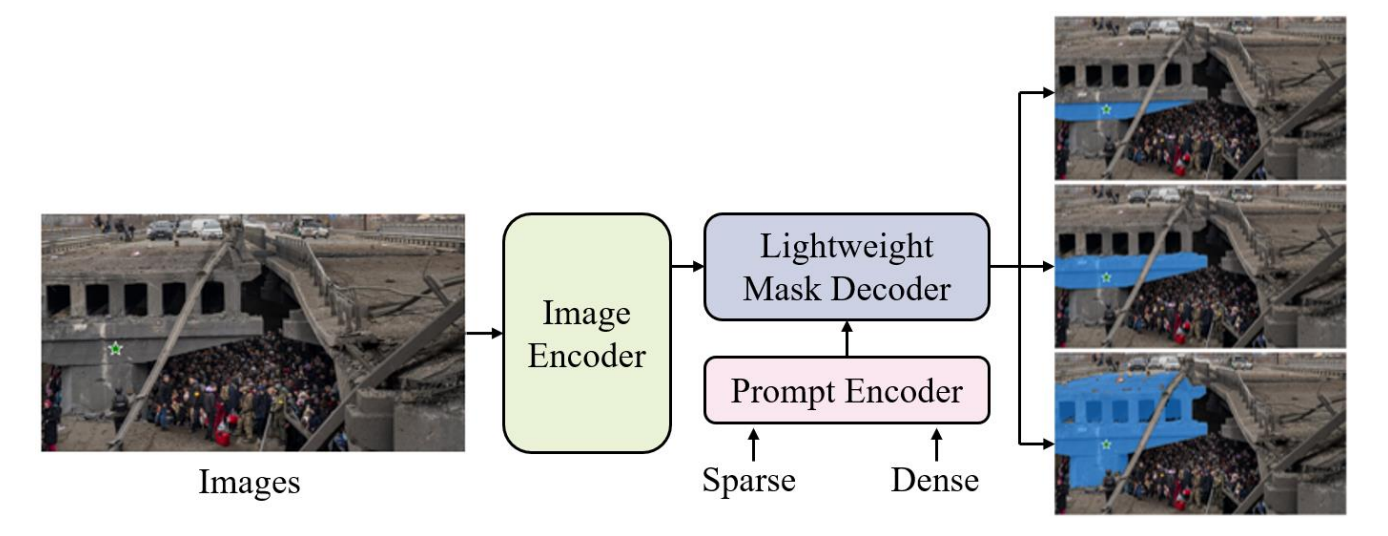
Following the lower section of the flowchart (*Figure 3*) the Coherence and CCD products are integrated into ArcGIS software for further analysis. In particular, at the **fourth phase (4)** CCD products are visualized to illustrate the sites with values that are potentially identified as damages. Specifically, the products of this phase highlight the changes between periods before and after the induced damage, providing a semi-automatic way of detecting major changes. Under this light, the coherence and CCD products are combined and mutually compared in order to focus in areas close to bridges and proceed to statistical analysis in an effort to highlight the damaged man-made environment. After rough assumption of coordinates of bridges under evaluation each of them is considered in more detail with the use of Google Maps and Setinel-1 images to exclude some of the assets, which did not meet the target of the research. The subset region in geographical coordinates using WKT-format is used to indicate area of interest of each assessed bridge. Then, the results are exported to ArcGIS environment for illustration and geographical collocation.

### 3.3. Component damage characterisation

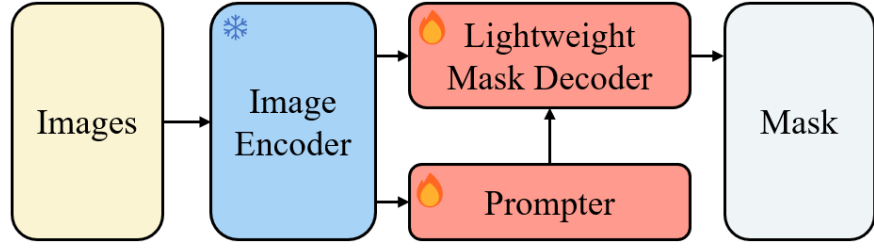
In this section, the component detection and automatic localisation and classification of damage using semantic segmentation is described from a methodological point of view and also illustrated in Figure 4. For assets, detected with high coherence values for which macroscopic remote sensing data is not adequate to make decision, further visual information is collected from the open platforms, such as Damage In UA and UADamage (see more in section 4). The images that have shown visible structural damages are then processed using selected CV techniques to automatically detect the condition of the components. For this, two steps are required: (i) component segmentation, for the detection of specific components of the structure; and (ii) instance segmentation, for the assessment of damage types for the component. As in some cases images are taken under adverse conditions that limit the image resolution, targeted techniques for image pre-processing based on large pre-trained foundational models are used to improve the quality of images and remove the occlusion. Applying these large pre-trained foundational models, as well as models pre-trained for image-text matching, like Contrastive Language-Image Pre-Training (CLIP) [75],

and Grounded Language-Image Pre-training (GLIP) [72], expanded the capabilities to downstream and customize our CV tasks.

All the image pre-processing of component damage detection has been performed based on state-of-the art model for instance segmentation - the Segment Anything Model (SAM) [69]. SAM project was introduced by MetaAI in 2023. Its core involves the establishment of a data engine, which comprises three stages: assisted-manual annotation, semi-automatic annotation, and fully automatic annotation, with refinements and improvements at each stage of the process [69]. This approach generated a massive 1.1 billion mask dataset (SA-1B), which is 400 times larger than existing segmentation datasets. Building upon this large-scale dataset, the Segment Anything Model (SAM) was designed with a heavyweight image encoder that generates image embeddings. These embeddings can be queried efficiently with various input prompts (points, box, and text) to generate object masks in real-time. The structure of SAM applied to segmenting of structural damage is shown in Figure 4 below.



(a) The architecture of the SAM model [69] includes an image decoder, a prompt decoder, and a lightweight mask encoder. The image decoder generates image embeddings, and the prompt decoder accepts two types of prompts: sparse (points, bounding boxes, text) and dense (masks) from human, converting prompts into prompt embeddings. The mask decoder generates corresponding masks based on both the image and prompt embeddings. The diagram illustrates an input with a point prompt (green star) on the main body of a bridge. SAM then generates three different masks corresponding to the whole, parts, and subparts of the bridge.



(b) The architecture of SAM-based RSPrompter with self-generating prompter [70]. This architecture replaces the prompt encoder with prompter which can receive output from the image encoder and extracting key features to train itself in generating the required prompts, enabling the algorithm to execute automatically. Heavy SAM's image encoder will be frozen and not participate in training.

Figure 4. (a) Segment Anything Model Overview [69]; (b) SAM-based RSPrompter with prompter [70].

SAM exhibits strong zero-shot generalisation capabilities in computer vision tasks. By employing a uniform scattering of points as prompts, SAM can perform edge detection on various parts of images, generating a multitude of masks autonomously. Besides, a suitable prompt can accurately generate the masks required by the user. As

shown in Figure 5, only two prompt points are needed to select the most matching mask, which is the crack in the figure that is used for component damage characterisation. In fact, prompts can also be automatically generated through appropriate training to achieve fully automated extraction of specified masks, and the obtained IoU (Intersection over Union) accuracy can maintain state-of-the-art levels compared with other instance segmentation models [70].

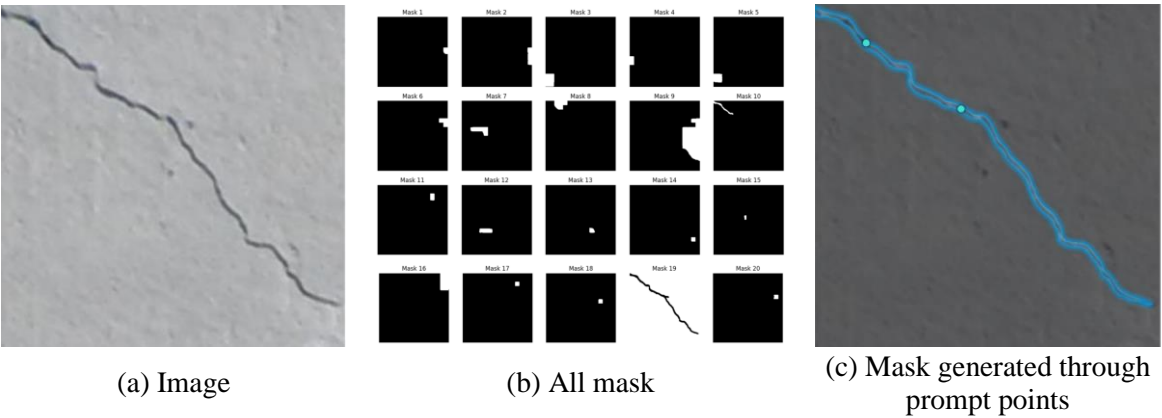


Figure 5 Generation of the mask required by the user through prompt points at component level

Additionally, SAM serves as a pre-trained foundational CV model that can generate masks with high quality, when combined with various downstream tasks or integrated with other large models. This has consistently demonstrated high performance compared to other state of the art models. In this paper, various image pre-processing techniques were employed to achieve component damage characterisation, one of which is Grounded-SAM. This method integrates Grounding DINO (self-distillation with no labels) [71] and SAM. Grounding DINO, built upon GLIP [72], is designed for open-set object detection. GLIP is a well-known project that trained by 27 million image-text pairs to establish the connection between image and text. SAM generates masks from input images and each of these masks are then automatically assigned tags/labels by Grounding DINO. This technology was found to recognise successfully common vocabulary such as bridges, road and cars. With regard to stable diffusion [76], this is also as a widely recognized image generation algorithm, a type of diffusion probabilistic model that involves iteratively refining a random noise vector to create realistic images. This technique is used in this paper for image inpainting, effectively eliminating occlusions that obscure our primary detected objects. Figure 6 presents our workflow diagram for automatic localization and classification of damage at component level.

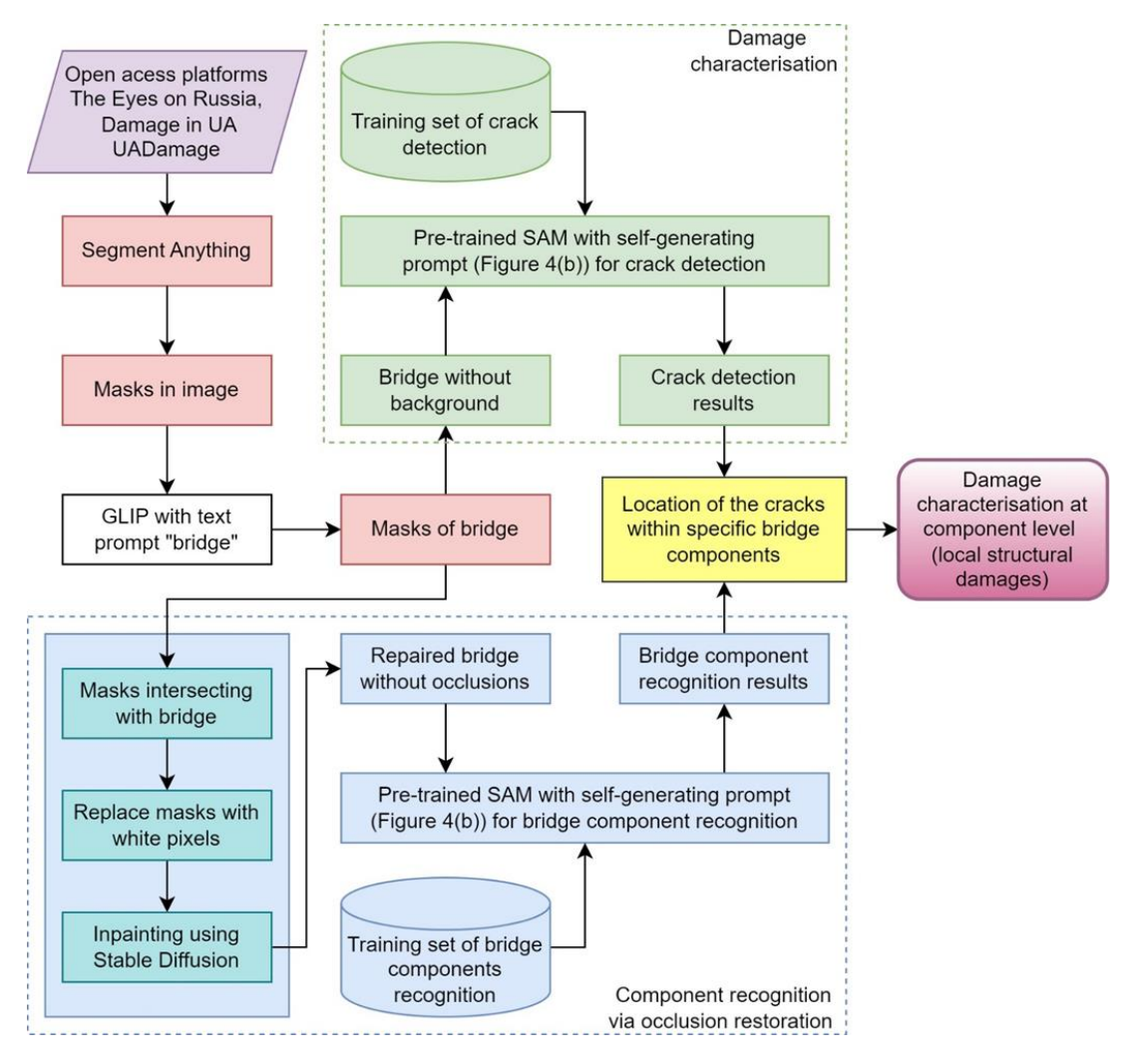


Figure 6. Flowchart, illustrating damage characterization at component level.

Starting with the selected images collected from open platform, the input first undergoes processing using SAM's everything mode to detect all potential masks present in the image. Subsequently, each mask is assigned labels, and those with the "bridge" label are singled out. Following this step, two distinct processes unfold: damage identification and occlusion restoration. The damage characterisation process utilizes the previously identified bridge masks, excluding all pixel except those within the bridge masks. Utilizing a pre-trained self-prompting SAM, it can automatically detect damage, such as cracks. The other process first captures masks intersecting with the bridge masks. These intersected masks are considered areas requiring treatment, employing stable diffusion for inpainting. This process generates the missing parts of the bridge structure due to occlusions. Subsequently, similar to the process of damage identification, another pre-trained self-prompting SAM automatically performs bridge component detection tasks based the repaired bridge image. Finally, the identification outcomes from both processes merge, enabling the determination of where the damages have occurred within the bridge components. This integration facilitates the damage characterisation detection of structural damages at the component level.

# 4. Analysis of the case study, results, and discussion

# 4.1. Description of the case study area

The case study was selected to be an inaccessible region, for which it is challenging to assess infrastructure damage and design restoration measures. Since the onset of the conflict in Ukraine, extensive destruction of civil infrastructure has taken place as a result of missile attacks, shelling and artillery fire. Roads and traffic have been extensively disrupted, as a result of damage of more than 345 bridges across the country [77]. This damage was more pronounced in the Kyiv region and in particular the bridges along the Irpin river were systematically damaged to disrupt connection routes, e.g. Bucha-Kyiv, Hostomel-Kyiv, Irpin-Kyiv. These bridges are particularly important because they serve logistic and supply routes, and facilitate evacuation of civilian population of the capital through humanitarian corridors (see Figure 7.). The critical role of the bridges in this region, their considerable damage and the fact that they are not accessible for assessment and decision-making due to the ongoing hostilities, gave the motivation for this case study (Figure 8). The aim of this case study is to identify and characterise the level of damage of selected bridges along the Irpin river, at asset and component level, by implementing the methodology described in section 3, to enhance the resilience of the area, when access and funds are made available. This reduces the reaction time of traditional time-consuming inspections that would normally take place when hostilities cease.

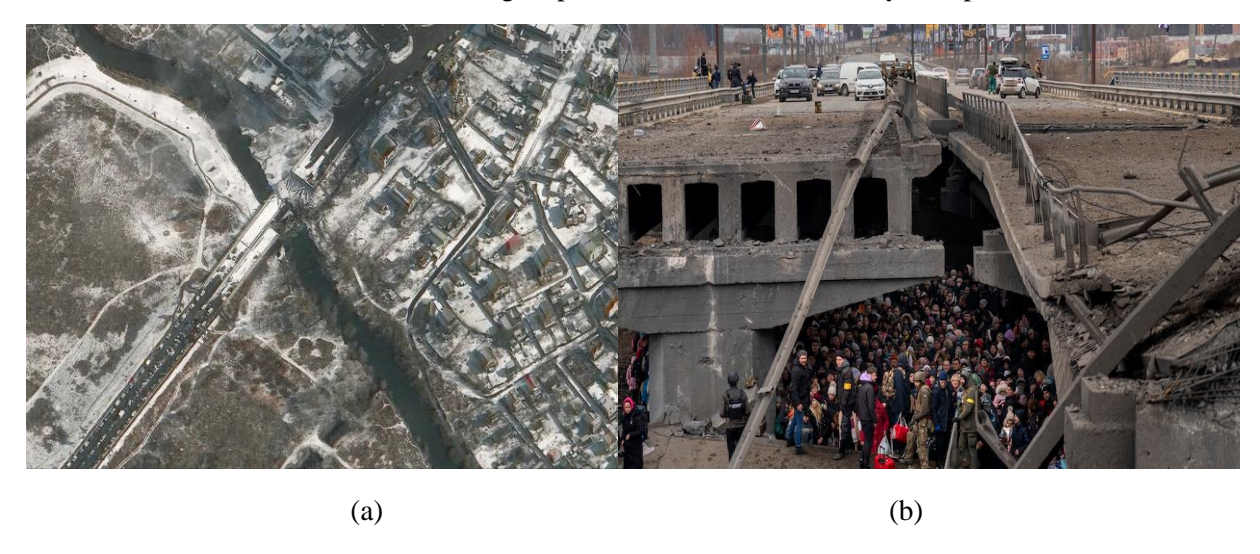


Figure 7. Examples of damage: (a) satellite imagery of bridge over the Irpin river captured by Maxar [80] and (b) bridge near Irpin city[81]

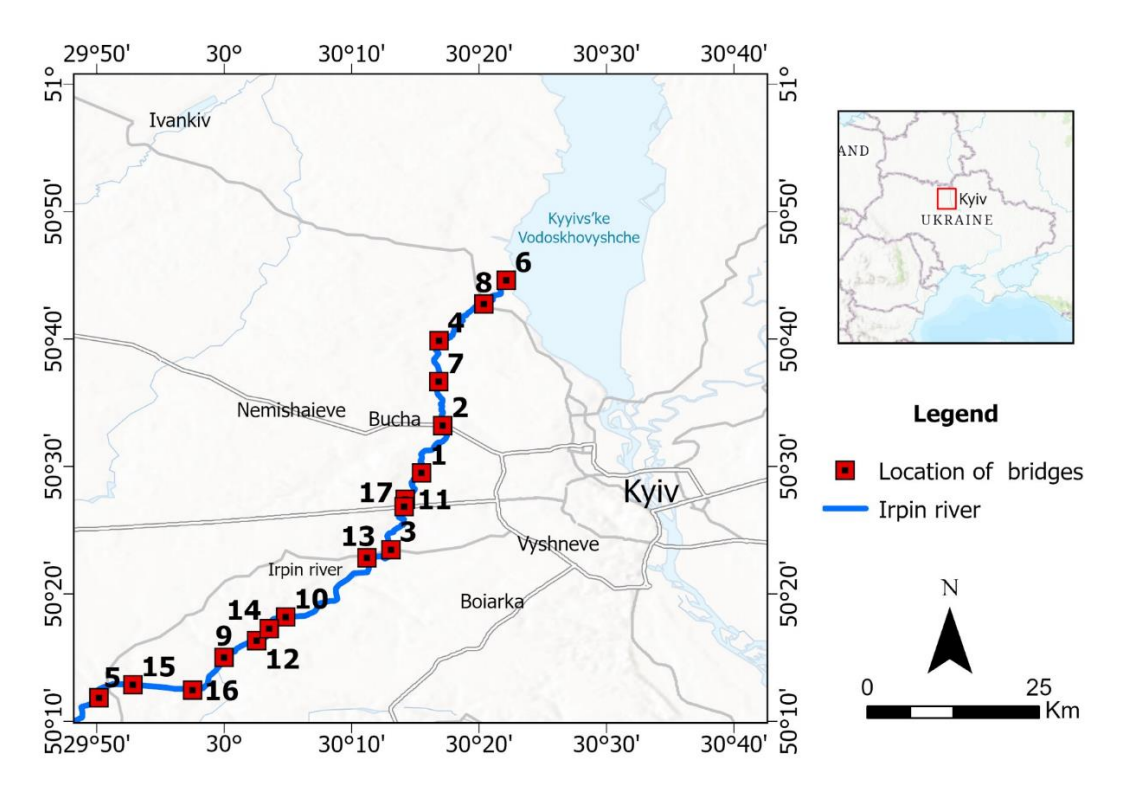


Figure 8. Study area (west of Kyiv). The numbers indicate bridges` ID, and the blue line illustrates the Irpin river.

#### 4.2. Regional and asset level assessment

Here the methodology for post-disaster damage characterisation at regional and asset level was employed (section 3.2). At the **regional level**, open geospatial data from OpenStreetMap were utilised to select the river crossing bridges that serve an essential connection, while alternative routes are sparse or unavailable due to the low redundancy of the network. In doing so, bridges that can be bypassed through alternative routes were not included in this analysis.

Bridges crossing the Irpin river in the area of interest were visually validated and geometrically corrected using and open access Google Satellite Imaginary and high spatial resolution optical images of the Maxar basemap in ArcGIS pro. Initially, a total of 24 assets (ID 1 to 24) was processed, which, according to OpenStreetMap seem to serve as bridges. Then, the coordinates of the assets were automatically identified for further localised analysis as per Table S.1 in Supplementary materials. The same table provides information about the structures examined, also openly available online on OpenStreetMap and Google Maps, including bridge types and their dimensions. Next, each asset was considered individually in detail, and Google Maps and Setinel-1 images were used and as a result some assets were excluded from the list. The ones excluded were assets with ID 18 to 21, which were confirmed to be hydraulic structures, thus, not serving as traditional bridges. The last filter applied was based on the length of the assets, and hence assets with ID 22, 23 and 24 were also excluded, due to very small size (<10m), hence, serving as culverts, which can be easily bypassed. After this filtering, a total of 17 bridges were analysed (assets with ID 1 to 17, see Table 1). Following this, the establishment of the study area was delineated at the west part of Kyiv, to select and download the appropriate radar images, which are then processed at the asset level.

Table 1. Application of post-disaster damage characterisation using Sentinel-1 SAR images at asset level

	Coheren	Coherence (2 $\sigma$ ) Coherence (Max)		e (Max)	CCD			
Bridge	Before	After	Before	After	$2\sigma$	Max	LKn	DL
1	2	3	4	5	6	7	8	9
B1	0.816	0.501	0.829	0.517	0.523	0.632	LKn <sub>H</sub>	DL <sub>H</sub>
B2	0.859	0.611	0.967	0.829	0.499	0.540	$LKn_H$	$DL_H$
В3	0.625	0.437	0.651	0.461	0.375	0.384	$LKn_{M}$	$DL_M$
B4	0.229	0.211	0.376	0.295	0.118	0.241	$LKn_L$	$DL_L$
B5	0.633	0.387	0.652	0.389	0.333	0.387	$LKn_{M}$	$DL_M$
B6	0.876	0.717	0.889	0.754	0.144	0.390	$LKn_H$	$DL_L$
B7	0.567	0.527	0.570	0.558	0.142	0.156	$LKn_{M}$	$DL_L$
B8	0.359	0.433	0.436	0.435	0.112	0.115	$LKn_L$	$DL_L$
B9	0.889	0.330	0.890	0.338	0.666	0.730	$LKn_H$	$DL_H$
B10	0.469	0.506	0.469	0.506	-0.145	-0.145	$LKn_L$	-
B11	0.588	0.526	0.588	0.526	0.280	0.280	$LKn_L$	$DL_L$
B12	0.504	0.446	0.526	0.456	0.188	0.189	$LKn_L$	$DL_L$
B13	0.406	0.346	0.505	0.401	0.087	0.178	$LKn_L$	$DL_L$
B14	0.406	0.231	0.505	0.313	-0.029	0.062	$LKn_L$	$DL_L$
B15	0.567	0.264	0.683	0.376	0.350	0.400	$LKn_{M}$	$DL_M$
B16	0.549	0.204	0.567	0.208	0.349	0.359	$LKn_L$	$DL_L$
B17	0.821	0.647	0.941	0.756	0.351	0.521	$LKn_{H}$	$DL_M$

At the **asset level**, SAR Single Look Complex (SLC) images of Sentinel-1 mission for the period of interest (time of military hostilities in Kyiv region) were used to detect and characterise damage. In order to produce the coherence products, three of Sentinel-1 mission interferometric wide swath (IW) SAR images were obtained in ascending and descending geometry (six in total) covering the time period from February 2022 to March 2022.

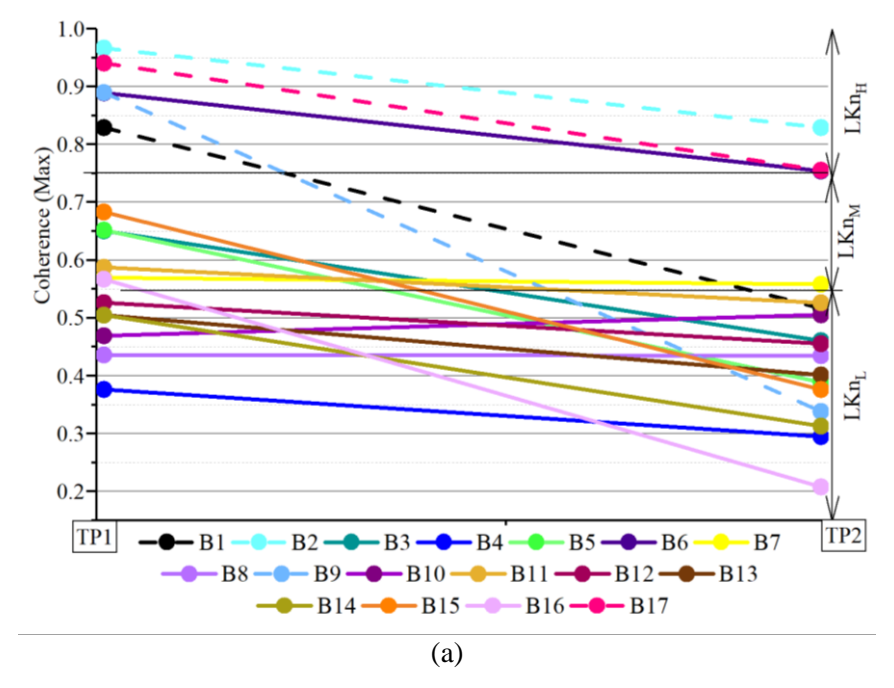
The Coherent Change Detection (CCD) approach is used for post-disaster damage assessment derived from the difference between the coherence products before (taken on 19/01/2022 and 12/02/2022, - time period 1 (TP1)) and after the onset of the war (taken on 12/02/2022 and 01/04/2022,- time period 2 (TP2)). Corresponding datasets for the period of the most extensive destruction of the analysed region was obtained with the use of open access platforms (e.g. Damage in UA [62], Eyes on Russia [63], UA Damage [64]), providing additional evidence regarding rhe affected assets for cross-validation of results at regional and asset levels and further damage characterisation at component level (see section 4.3. for more details).

Positive values of CCD represent plan view areas of the asset that demonstrate significant differences, possibly corresponding to significant displacements and hence damage of bridge decks. Small values, closer to zero, correspond to areas that represent smaller deformability of the asset, as recognised by subsequent satellite passes, thus inferring areas of no or minor damage. Negative values are related to the appearance of new stable areas, during the interval between the two coherence products. Changes in coherence within two pre-damage and two pre- and post-damage images were employed for characterising the level of asset damage (see section 3.2). Table 1 contains the results of the maximum values of coherence between each pair of images as per columns 4 and 5, and values, with lower dispersion from the mean in the analysed area as per columns 2 and 3. Thus, "2σ-adjusted" coherence results indicate the range, for which 95% of the data is within two standard deviations of the mean. Similarly, columns 6 and 7 show the maximum and "2σ-adjusted" CCD values between two pairs of images. If translated into damage characterization, maximum CCD values correspond to the highest change of coherence, identified at the

area of asset, which could be analogized with high localized destruction on the bridge. In contrast, "2σ-adjusted" CCD values correspond to the averaged destruction within the area of the analysed structure (e.g., the damage level is lower, but covers bigger part of the bridge).

As the use of Setinel-1 low resolution images provides limited opportunity for accurate identification of damage level, for some of the assets the resolution of images was not sufficient, because the coherence values were very low for the pairs of the images examined. However, for some structures the proposed approach has demonstrated the outstanding capability of damage assessment in limited access conditions. All assets were classified by the Level of Knowledge (LKn) that reflects the degree of reliability of results, according to image resolution and the coherence between image pairs. These pairs of images, for which coherence results before the hazard occurrence were high, were assumed to be of higher reliability. Thus, structures were classified in groups of low (LKn<sub>L</sub>), medium (LKn<sub>M</sub>), and high (LKn<sub>H</sub>) reliability. Also, according to CCD values, each asset was assigned with an index, linked to its damage level (DL), i.e. DL<sub>L</sub> (low), DL<sub>M</sub> (moderate), DL<sub>H</sub> (high). Numerical values are given in Table 1 and additional illustrations of LKn and DL indexes are provided in Figures 9 to 11. These figures identify a general trend of reduction of coherence values for all bridges studied. both, damage level and the degree of reliability of results were different.

The damage level of a bridge can have a significant impact on both its functionality and the costs associated with restoration. The extent of damage directly influences the structural integrity of the bridge. Damage level is a vital parameter, identifying the load-bearing capacity of the bridge, thus, causing restrictions on traffic loads or, in severe cases, a complete closure to prevent safety hazards, which could be the crucial factor for overall stability of transport infrastructure in the region. Also, the more extensive the damage, the higher the loses, associated with restoration, including direct and indirect. Structural repairs, replacement of damaged components, and rehabilitation efforts contribute to the overall expenses, which could be summarized as the direct costs. The duration of the restoration process is another crucial factor for the functionality of logistic routs of the region, as extended downtime affects the functionality of the bridge and may lead to indirect economic losses for the surrounding area. In this context effective preliminary assessment of the damage level of structures, in regions with limited access to them, facilitates remote restoration planning and decision making.



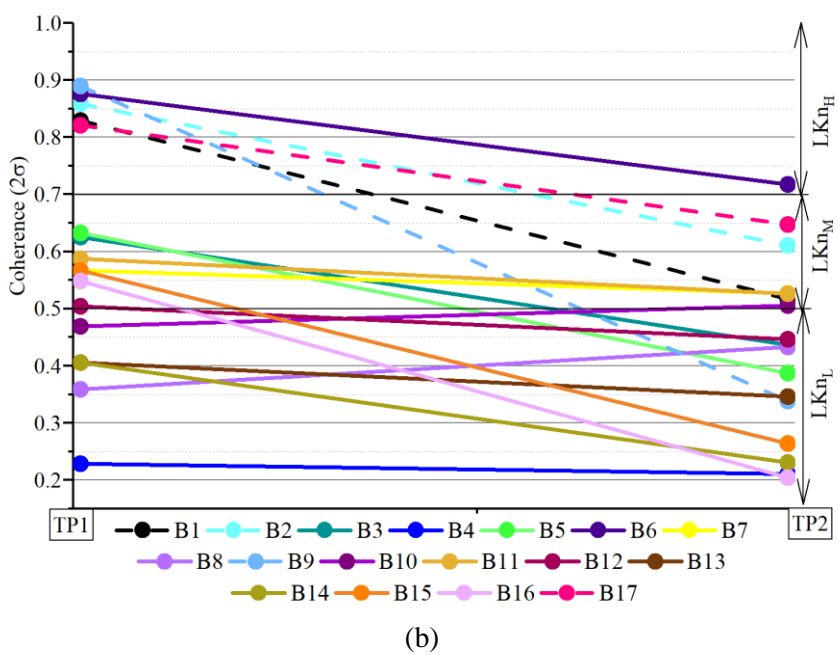


Figure 9. Change of coherence values within the estimated period (before and after the damage): (a) maximum values, (b) 2σ-adjusted values. Dashed lines depict the bridges with highest coherence changes. Maximum CCD values correspond to the highest change of coherence, identified at the area of asset (e.g. high localized destruction on the bridge), while "2σ-adjusted" CCD values correspond to the averaged destruction within the area of the analysed structure. Time period 1 (TP1) includes temporal dataset before the beginning of destruction (between 19/01/2022 and 12/02/2022), while time period 2 (TP2),-during extensive hostilities (between 12/02/2022 and 01/04/2022).

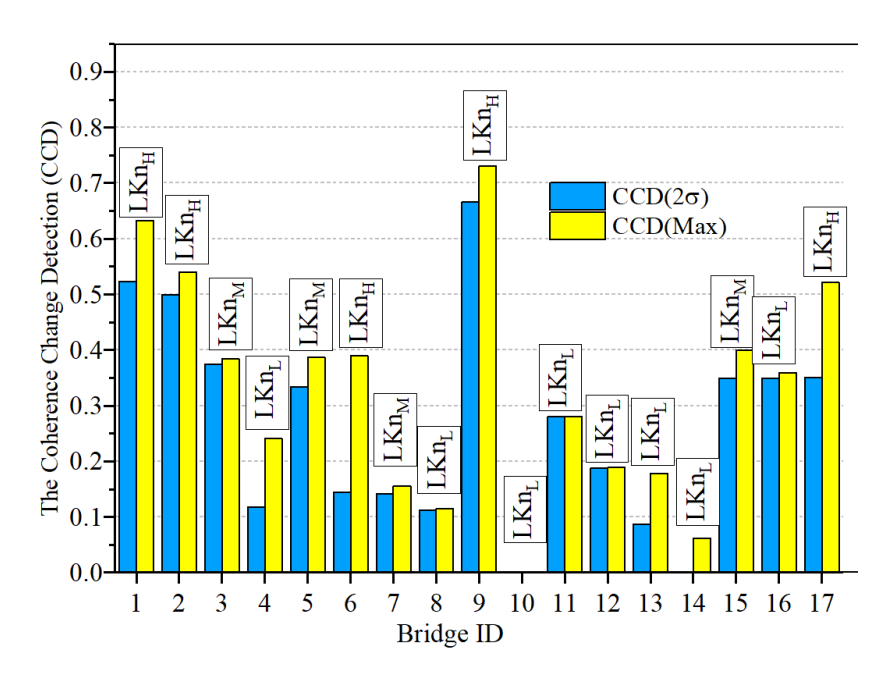


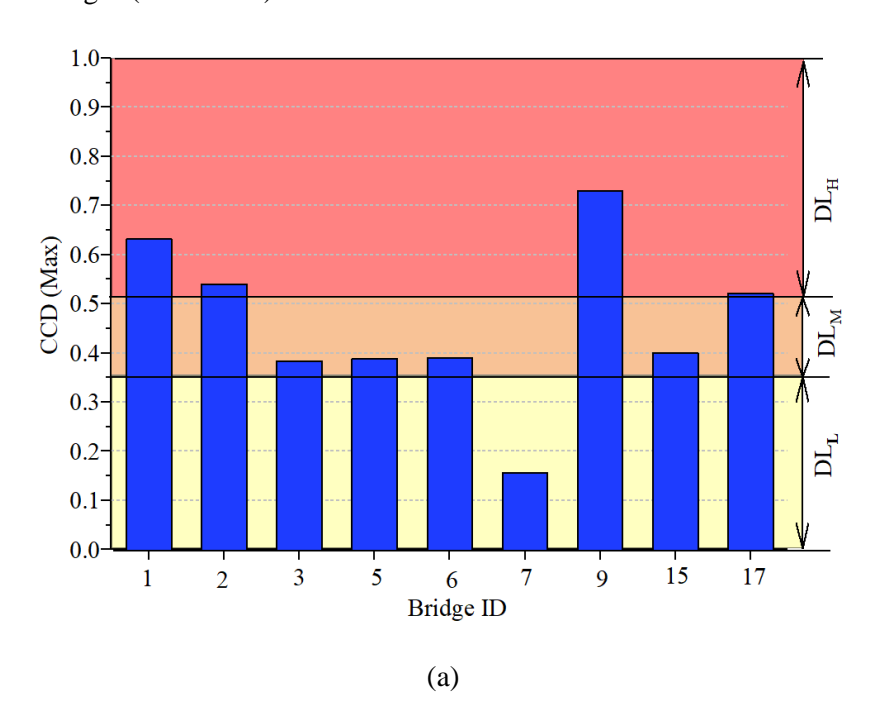
Figure 10. CCD values (as the indicator of coherence changes between two time periods) and level of reliability of information for the bridges studied: Maximum CCD values correspond to localized destruction on the bridge, while "2σ-adjusted" CCD values correspond to the averaged destruction within the area of the analysed structure.

The data obtained at this stage should be considered with caution relative to the level of evidence about the quality and accuracy of the results. This is because not all the results are representative for bridge post-disaster damage characterisation at asset level. For this, a LKn was defined to exclude assets for which the information is not adequate or of the desired accuracy (see figures 9-10, where different ranges of reliability are clearly indicated). Thus, based on engineering expert judgment approximate ranges were assumed and introduced for classification of bridges according to the degree of reliability at asset level (see Table 2).

**Table 2.** Classification of objects according to the degree of reliability

LKn	Coherence (Max)	Coherence (2σ)
LKn <sub>H</sub> (High)	0.75-1	0.7-1
LKn <sub>M</sub> (Medium)	0.55-0.75	0.5-0.7
$LKn_L$ (Low)	0-0.55	0-0.5

For further analysis bridges with the low LKn evidence, were neglected, as this data could not be reliable for making assumption about the level of damage, for instance, B4, B8, B10- B14, B16. Figure shows the interferometric coherence difference values for the remaining examined bridges. CCD values can be used as the identifier of how much the period of missile attacks during February-March 2022 resulted in deterioration of bridge structures in Irpin region. In particular, these structures can be grouped according to the level of damage (DL) with the use of approximate ranges (see table 3).



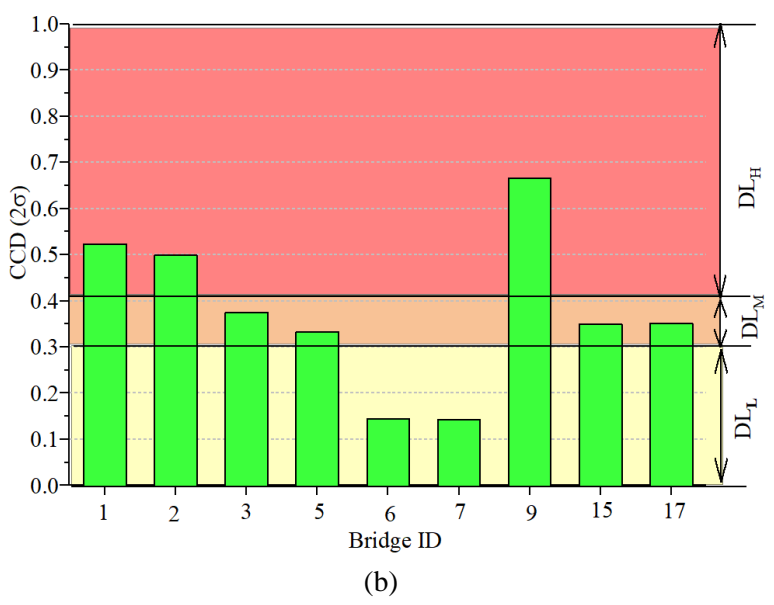


Figure 11. CCD values within the estimated period (before and after the disaster): (a) maximum values, corresponding to localized destruction on the bridge, (b) 2σ-adjusted values, indicating the averaged destruction within the area of the analysed structure.

Table 3. Damage characterisation of infrastructure assets (bridges) based on CCD.

DL	CCD (Max)	$CCD(2\sigma)$	Colour legend	Description
DL <sub>H</sub> (High)	0.5-1	0.4-1		Total destruction of whole structure or some of the
				components. This corresponds to Severe/Complete
				damage.
$DL_{M}$ (Moderate)	0.35-0.5	0.3-0.4		Considerable damage in some of the components.
				This corresponds to Moderate/Extensive damage.
DL <sub>L</sub> (Low)	0-0.35	0-0.3		General deterioration, signs of slight damage This
				corresponds to Minor damage.

As was mentioned above, the results of Coherence Change Detection method in different scales indicate different types of destruction in assets. Thus, the maximum coherence changes (CCD(Max)) illustrate the highest changes within its area, occupying only minor its portion which serves as an analogue of local destruction (e.g. 1 span of three-span bridge, or one structural element being completely destroyed, while others are unaffected). The  $2\sigma$ -adjusted values, in contrary, are associated with average coherence difference, prevailing on the largest area of the asset. For instance, low or medium CCD ( $2\sigma$ ) results can indicate general deterioration of the bridge: road pavement damage, concrete crushing, and spalling, etc. Therefore, different levels at both " $2\sigma$ " and "Max" scales could serve as the prerequisite for evaluation of remaining capacity of the bridge, both structural and traffic. For additional illustration of such scales, and comparative analysis, - see Figure 12.

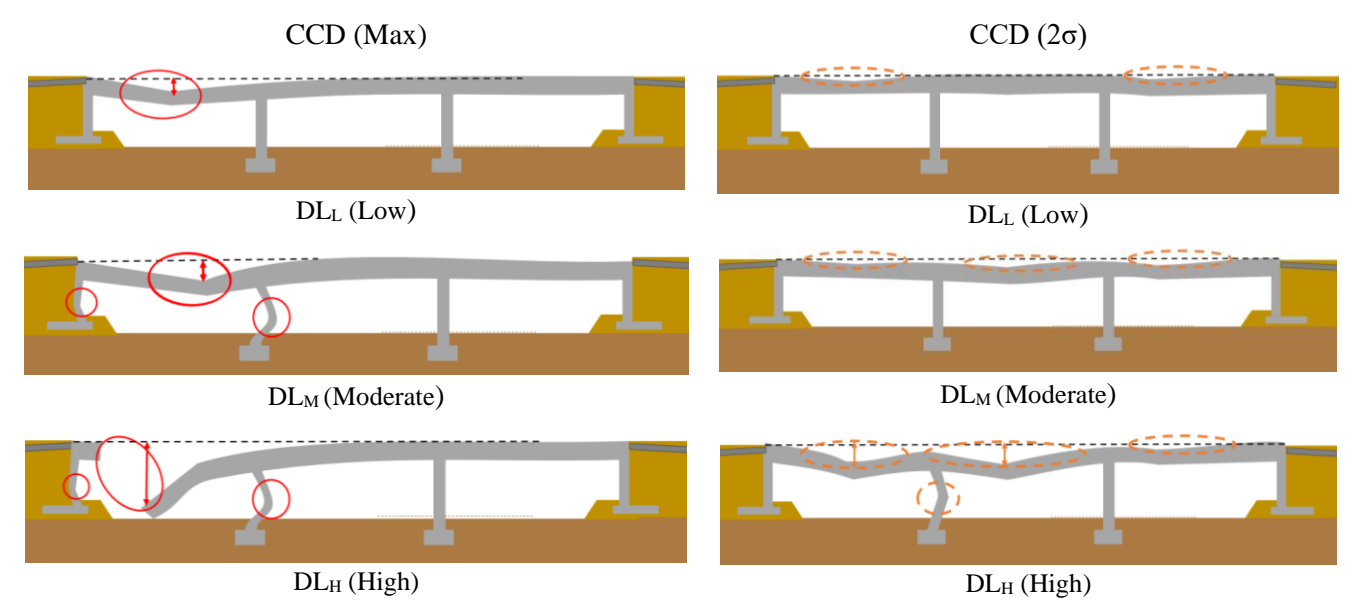
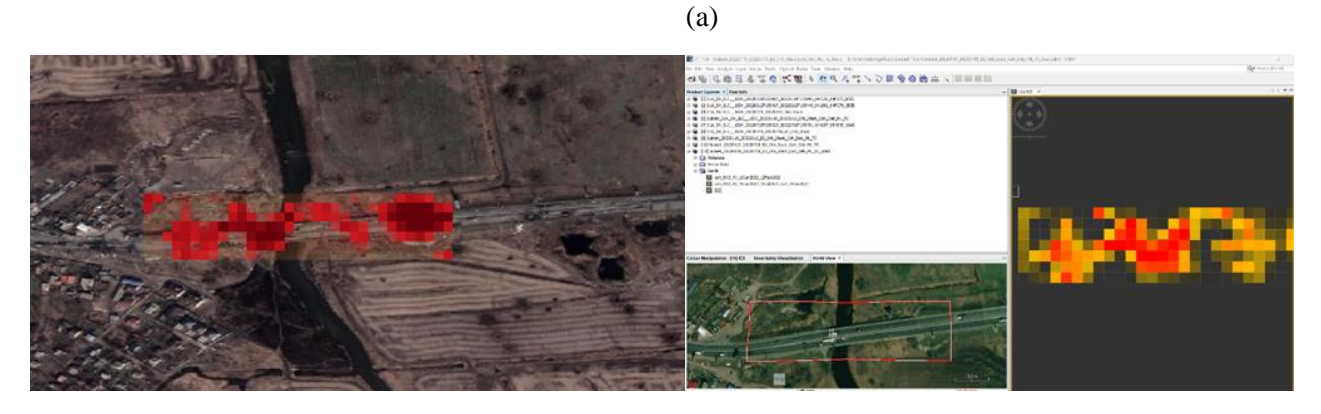


Figure 12. Illustration of different types of damage level (DL), indicated via maximum CCD and 2σ-adjusted CCD damage detection. Red continuous lines indicate CCD(Max) values, corresponding to local damages and orange dashed lines outline CCD(2σ) values, associated with average general deterioration of the bridge.

CCD values were transferred to QGIS software for visualization of damages at different levels of reliability (see Supplementary materials, Fig. S.1-S.3). Illustrations of damage detection for assets which demonstrated the highest capability of the proposed approach ( $LKn_H$ ) and have the most extensive destruction ( $DL_H$ ) are given below (See Fig. 13).





(b)



(c)



Figure 13 Damage characterisation at asset level for assets, demonstrating High LKn and High DL: (a) B1, (b) B2, (c) B9, (d) B17. (For additional results for bridges with Low and Medium DL, - see Supplementary materials)

The utilization of open-access platforms for the detection of damages in assets during war is a strategy that leverages freely accessible and publicly available resources to assess and monitor the impact of conflict on infrastructure. The transparency and complete availability of information from such platforms to the public nowadays, significantly contributes to accountability and a more comprehensive understanding of the situation in conflict-prone zones. Although, this data may differ in quality and may require verification, as crowdsourced data can sometimes be subjective or unverified, the combination of different sources enhances reliability. For instance, the cross-validation applied in this research entails the comparison of the CCD damage characterisation results outlined above with the high spatial resolution images from Google Earth Pro. This sources, as an example of an open-access platform, provides geospatial data that can be crucial for mapping and understanding the geographical extent of damages. It includes details about roads, buildings, and other infrastructure. Such additional optical validation of the results with high spatial resolution satellite images obtained via Google Earth Pro is demonstrated below (see Figures 14). Specifically, the left images are captures before the damage, while the right images are from March and April of 2022. Thus, visual comparison between photos of assets, obtained before the beginning of hostilities (October, February 2022) and after the period of the most extensive destruction in the region (April, March 2022) demonstrate considerable correspondence with evaluation results from approach outlined above.







(c) B9



(u) D1/

Figure 14. High spatial resolution images from Google Earth pro, which validate the damage to bridges B1, B2, B9 and B17 as detected by the Sentinel-1 coherence and CCD products.

Lastly, during the analysis, difficulties and limitations were identified related to the following issues:

**Spatial resolution of the satellite:** The Sentinel-1 has a spatial resolution of 20 m×5 m, resulting in which difficulties on the detection of small bridges. This problem can be overcome by utilizing high spatial resolution images from commercial satellite missions. However, there are limitations regarding the cost and the availability of those images. Particularly, the CCD products are based on pre- and post-event SAR images, and they cannot be generated when pre-event images are not available. This highlights the importance of having access to SAR images acquired before the event. Unfortunately, in many cases, commercial satellite missions acquire images in response to demand, which means that obtaining pre-event SAR images could not be possible. Consequently, this limitation affects the utilization of high spatial resolution images for bridge damage detection.

**Sequence of events:** During this specific time period, the environment was dynamically changing every day due to the disasters. It is crucial to know the timing of the damage so that we can have images before the event. Such aspect could be eliminated with the integrated utilization of open-access platforms, as outlined in this research.

**Line of sight:** The satellite captures the Earth's surface from a specific angle, which affects how geometries are depicted on the Earth's surface. In the following example (Figure 15 (a)), the same area is shown from a different angle using optical data (Google Earth Pro). The same phenomenon applies to radar data (Figure 15 (b)), but it is much more challenging to identify what is actually observed.



Figure 15 Impact of change of line of site, causing challenges in remote damage detection: (a) optical data (Google Earth Pro), (b) radar data.

Conclusively, based on the results examined in this study, the following issues were addressed:

• identification of damaged bridges and characterization of level of damage in conditions of limited access to the area of interest

The results of this study indicate that the use of Sentinel-1 SAR SLC images could provide outstanding for the identification of damaged bridges in context of limited access to data with higher quality (e.g. Sentinel-2). However, the size of the bridge should always be considered, as the method described herein is most applicable to structures of substantial size. The results suggest that the utilization of Sentinel-1 radar products is conducive to preliminary characterization of damage for assets with lengths exceeding 80-90 meters. However, it is important imperative to acknowledge the specificities of individual case studies, including the potential impact of weather conditions, precipitation, and seasonal variations, all of which may introduce distortions to the results. Another critical consideration in radar data-based assessments is the dynamic nature of environmental changes, leading to coherence variations unrelated to damages. Therefore, the precise timing of the damage event and the utilization of Sentinel-1 products closest to the assumed event date emerge as pivotal factors. Additionally, the use of images captured from the same satellite angle ensures that the line of sight does not impact the depiction of the geometry of assessed objects on the Earth's surface.

• comparison of data from different open access sources (OpenStreetMap, Google earth Pro, social networks, open access platforms, crowdsourcing) for obtaining additional information and validation of results.

The use of high spatial resolution images (Figure 16) such as the basemap of the Maxar images in ArcGISpro could be sufficient approach for comparison and validation of results and supplementation of data in conditions of limited access.



Figure 16, Examples of faulty digitized vector lines from OSM network.

Thus, although additional information (number of spans, visible columns, material) can be extracted from commercial satellite images with high spatial resolution (such as 30 cm), the role of open-access data is still a topical issue. Nonetheless, the availability of pre-event SAR images from commercial sources is not guaranteed, as these missions operate on a demand basis. Moreover, in conflict-related case studies, obtaining commercial satellite images during the conflict is often impeded by sensitivity concerns. Also, as shown by transition from regional and asset level to component level effectively demonstrates how open-access platforms could serve as reliable source for more detailed assessment of damaged asset.

# 4.3 Component level assessment

Damage characterization at component level was done for the bridge with the highest level of reliability of results and highest damage level. For the assessment of damages at the component level open access platforms Damage In UA [62], The Eyes on Russia [63] and UADamage [64] were used, which aim to collect, verify and integrate information, relating to the conflict in Ukraine. The Eyes on Russia, developed by The Centre for Information Resilience (CIR) and coordinated research with OSINT (Open Source Intelligence) including Bellingcat and GeoConfirmed platforms, provides reliable, verified, trustworthy and timely information about the impact of war circumstances on Ukrainian civil infrastructure, buildings, structures and people[63]. Damage In UA, implemented by the Kyiv School of Economics in cooperation with the Office of the President of Ukraine, the Ministry of Economy, the Ministry of Reintegration of the Temporarily Occupied Territories, and the Ministry of Infrastructure of Ukraine collects, analyses and asses information, provided by the government, local authorities, public sources, as well as high-precision drone images and satellite data from Maxar Technologies (US government) [62]. UA Damage [64] initiative similarly provides database on infrastructural loses, obtained from satellite imaginary and computer vision. Thus, these open-access platforms were used to obtain links to trustworthy sources with images of bridge for damage detection at component level.

Using the methodology described in Section 3.4, for the selected Bridge 1, two automated CV tasks were performed:

- Instance segmentation of affected bridges for component detection and classification
- Instance segmentation for defect detection, location and classification for the following categories (e.g. Crack)

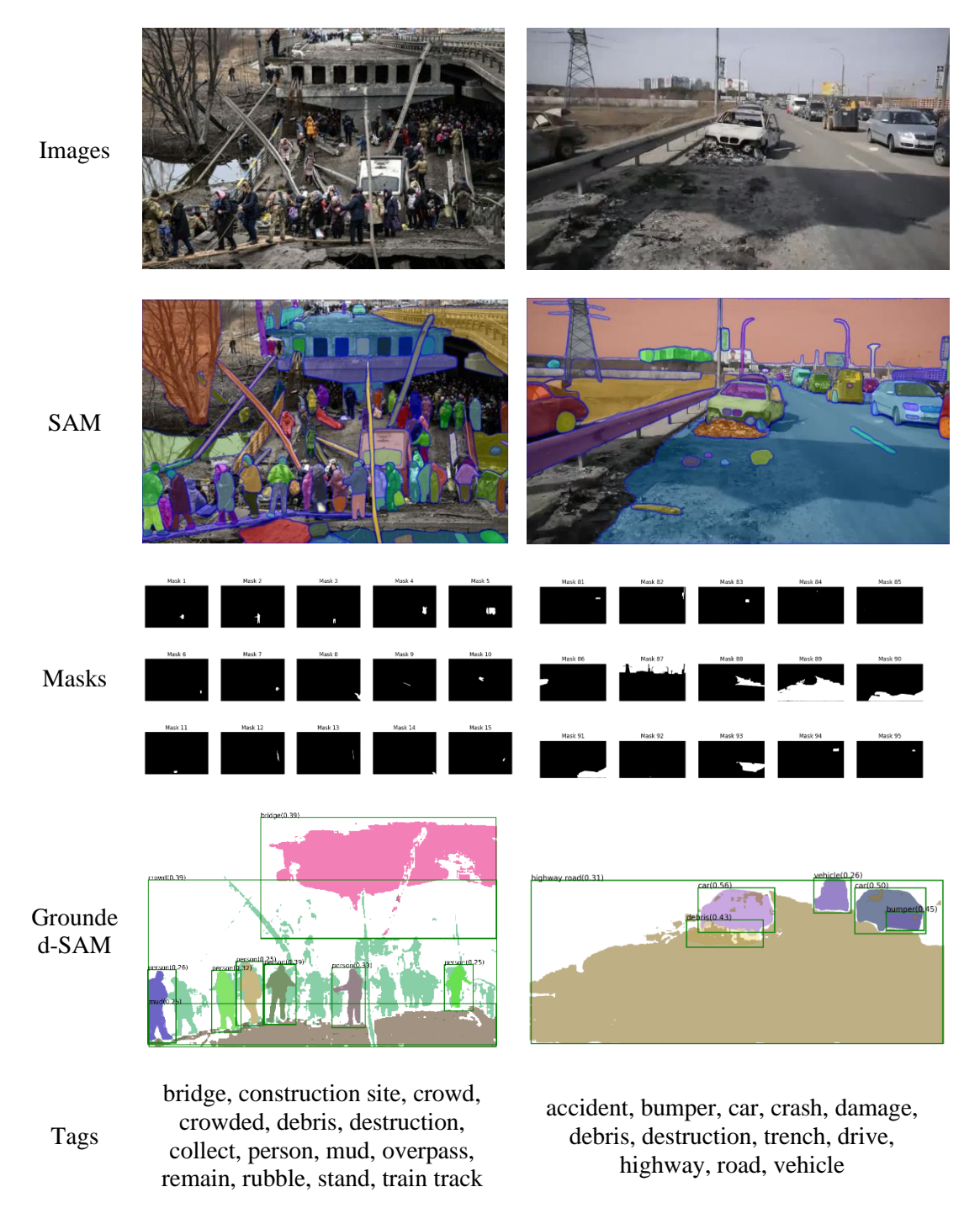


Figure 17. The outputs of SAM and Grounded-SAM

The outputs of SAM and Grounded-SAM are shown in Figure 17. Firstly, the input images undergo mask extraction using SAM's everything mode. The visual representation of SAM's segmentation results is showcased in the second row, while the individual mask outcomes are presented in the third row. Subsequently, employing Grounding DINO [71], labels were matched with the obtained masks, excluding masks below the recognition threshold from display, and the results are displayed in the Grounded-SAM row. Additionally, all labels extracted from the masks, and some other descriptive words from Grounding DINO are presented in the 'tags' row.



(a) Image



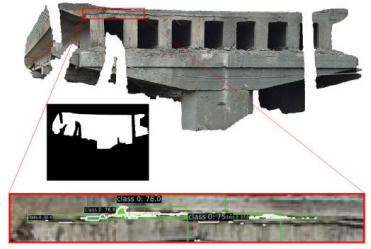
(b) SAM Result



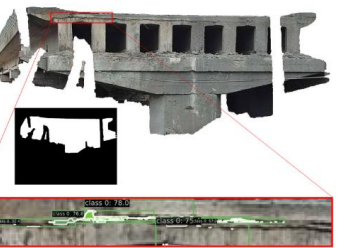
(c) Grounded-SAM (general detection)

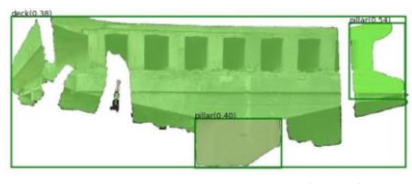


(d) Stable Diffusion for Occlusion Repair

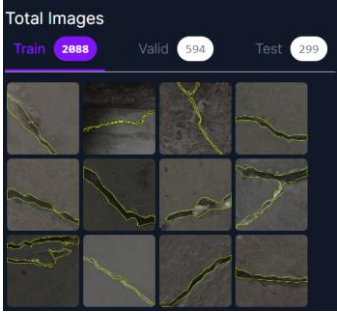


(e) Bridge Capture and Crack Detection

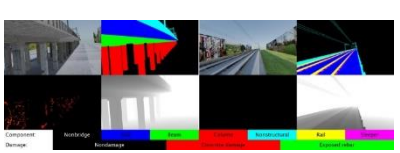




(h) Instance Segmentation for Component Level based on SAMgenerated mask



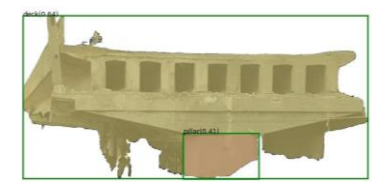
(f) Training Set for Crack Detection [75]



(i) Training Set for Component Level Detection (Tokaido dataset [74])



(g) Bridge Capture



(j) Instance Segmentation for Component Level based on Repaired SAM-generated mask

Figure 18. Combined component and damage detection for the bridge B1

In contrast to the common bridge component recognition research, severe damage conditions introduce two complex challenges: firstly, the background for detection becomes highly intricate, and secondly, there is uncertainty of occlusion affecting the bridge (see Fig. 18 (a)). Therefore, Grounded-SAM is initially employed for an initial general detection task (Fig. 18 (b)), with the objective of identifying the specific mask corresponding to the bridge (see Fig. 18 (c)). Subsequently, the bridge subject is extracted from the image, and any remaining areas are replaced with a white mask (Fig. 18 (e)). At the same time, the masks intersecting with the bridge are filtered, pixels within these masks are removed, and Stable Diffusion is employed to fill in the erased areas (Fig. 18 (d)). This process effectively eliminates intricate backgrounds and occlusions unrelated to the bridge subject. The repaired bridge mask is extracted from the background once again (Fig. 18 (g)).

The extracted bridge that has not been repaired will carry out crack detection task using a dedicated mode. This crack detection model has been trained on a dataset of approximately 3000 images (Fig. 18 (f)) and utilizes the query-based learnable prompt SAM algorithm mentioned in section 3.4 [70] as shown in Fig. 18 (e). On the other hand, the occlusion repaired bridge will undergo bridge component detection tasks. The model employed here is also self-prompting SAM, trained on the Tokaido dataset [74] illustrated in Fig. 18 (i). As shown in Figure (h) and (j), the component detection result significantly improves after the occlusion repairs. Finally, upon completing both the crack detection and bridge component recognition tasks, a simple matching process will be carried out to determine the location of the cracks within specific bridge components. This approach enables damage detection based on the level of bridge components.

# 5. Conclusions

The study on damage characterization using stand-off observations for recovery in the face of agnostic hazards, particularly those arising from targeted attacks, unveils critical insights and challenges in ensuring the resilience of infrastructure. Comprehensive multi-level research, presented in the article reveals a significant knowledge gap in remote detection and characterization of damage in bridge structures, which is of paramount importance for recovery planning, prioritization, and decision-making in conflict-prone regions. In particular, the topicality of the research is amplified for practical applications in post-conflict damage assessment scenarios in which immediate access to the on-site data is not possible. This cause considerable downtime extension, delays in restoration of infrastructure functionality and significant indirect loses. This study represents a pioneering effort in integrating information from diverse sources and leveraging emerging technologies tailored for specific purposes to assess bridge damage across various scales, encompassing component, asset, and regional levels. The methodology is implemented through a case study conducted in Ukraine, utilizing Sentinel-1 Synthetic Aperture Radar (SAR) images, crowdsourced data, semantic segmentation of images, and deep learning techniques.

In particular, Sentinel-1 Single Look Complex (SLC) products and OpenStreetMap (OSM) data obtained within the relevant timeframe were utilized at regional and asset levels for preliminary assessment of extent of damage and identification of assets with higher probability of being destroyed. The coherence between two pairs of images served at this stage as a metric for similarity in interferometric Synthetic Aperture Radar (SAR) returns from different acquisition dates. It was assumed, that changes in coherence (CCD) between two pairs of Sentinel-1 products could be considered as an indicative measure of the degree of damage (Level of Damage - LoD), with heightened CCD values presumed to correspond to areas exhibiting substantial deterioration. While the prevailing trend of decreasing of coherence values during the period of extensive bombarding is observed, the reliability of these outcomes exhibits significant variability. Thus, the level of certainty regarding the quality and precision of these findings (Level of Knowledge -LoKn) was implemented to exclude potentially low-quality results. The principal findings underscore the advantageous use of entirely open-access and remote data for the evaluation of structural damages. This assumes particular significance in scenarios characterized by limited accessibility, as exemplified in the case study of bridge destruction in Ukraine during the conflict.

For component-level damage characterization, the main challenges are complex backgrounds and uncertain occlusions in post-disaster images, affecting recognition accuracy. By combining advanced computer vision techniques, mask of bridge main body was extracted and occluded area was repaired, significantly improving the accuracy of defect recognition and localization for each bridge component.

Integrating stand-off observations and open-access information from diverse sources into recovery planning enables a more informed and adaptive response to agnostic hazards, facilitating expeditious decision-making processes for infrastructure development and the formulation of restoration strategies. The integration of novel approaches to assessment and damage characterization at different detalization levels with the use of stand-off observations and disparate sources provides perspectives for further application to another fields and case studies.

Consequently, it furnishes valuable insights to recovery mechanisms, encompassing decision-makers, governmental bodies, and funding entities, enabling them to judiciously prioritize investments.

Comprehensive understanding of stand-off damage to bridges is essential for developing effective design strategies, risk assessments, and mitigation measures to enhance the security and longevity of critical transportation infrastructure.

# Readers are encouraged to refer to Supplementary materials.

#### Acknowledgements

The first author would like to acknowledge the financial supports from British Academy for this research (Award Reference: RaR\100770). Several maps included in this work were created using ArcGIS® software by Esri. ArcGIS® and ArcMap<sup>TM</sup> are the intellectual property of Esri and are used herein under license. Copyright © Esri. All rights reserved. For more information about Esri® software, please visit https://www.esri.com/en-us/home (accessed on 15 December 2023). The authors are grateful to the European Space Agency and the National Aeronautics and Space Administration, who provided Sentinel-2 and SRTM data accordingly.

#### **CRediT** authorship contribution statement

Nadiia Kopiika: Methodology, Validation, Formal analysis, Investigation, Writing – original draft, review & editing; Andreas Karavias, Pavlos Krassakis: Conceptualization, Methodology, Writing –review & editing; Visualization; Nataliya Shakhovska: Conceptualization; Zehao Ye: Methodology, Formal analysis, Investigation, Writing – original draft, Visualization; Jelena Ninic: Conceptualization, Methodology, Writing – original draft, Supervision; Sotirios Argyroudis, Stergios-Aristoteles Mitoulis: Conceptualization, Writing –review & editing, Supervision; Nikolaos Koukouzas: Conceptualization .

#### **Declaration of Competing Interest**

The authors declare that they have no known competing financial interests or personal relationships that could have appeared to influence the work reported in this paper.

#### References

- [1] Sacks R, Kedar A, Borrmann A, Ma L, Brilakis I, Hüthwohl P, Daum S, Kattel U, Yosef R, Liebich T, Burcu Barutcu BE, Muhic S. SeeBridge as next generation bridge inspection: Overview, information delivery manual and model view definition. Automation in Construction, 2018; 90: 134-145. <a href="https://doi.org/10.1016/j.autcon.2018.02.033">https://doi.org/10.1016/j.autcon.2018.02.033</a>
- [2] Mitoulis SA, Argyroudis SA, Panteli M, Fuggini C, Valkaniotis S, Hynes W, Linkov I. Conflict resilience framework for critical infrastructure peacebuilding. Sustainable Cities and Society, 2023; 91, 104405. <a href="https://doi.org/10.1016/j.scs.2023.104405">https://doi.org/10.1016/j.scs.2023.104405</a>
- [3] Macchiarulo V, Milillo P, Blenkinsopp C, Giardina G. Monitoring deformations of infrastructure networks: A fully automated GIS integration and analysis of InSAR time-series. Structural Health Monitoring, 2022; 21(4), 1849-1878. https://doi.org/10.1177/14759217211045912
- [4] Giordano PF, Quqa S, Limongelli MP. The value of monitoring a structural health monitoring system. Structural Safety, 2023; 100, 102280. <a href="https://doi.org/10.1016/j.strusafe.2022.102280">https://doi.org/10.1016/j.strusafe.2022.102280</a>

- [5] Catbas N, Avci O. A review of latest trends in bridge health monitoring. In Proceedings of the Institution of Civil Engineers-Bridge Engineering, 2022; 176(2), 76-91. <a href="https://doi.org/10.1680/jbren.21.00093">https://doi.org/10.1680/jbren.21.00093</a>
- [6] Dong C, Li L, Yan J, Zhang Z, Pan H, Catbas F N. Pixel-level fatigue crack segmentation in large-scale images of steel structures using an encoder–decoder network. Sensors, 2021; 21(12), 4135. https://doi.org/10.3390/s21124135
- [7] Nettis A, Massimi V, Nutricato R, Nitti DO, Samarelli S, Uva G. Satellite-based interferometry for monitoring structural deformations of bridge portfolios. Automation in Construction, 2023; 147, 104707. <a href="https://doi.org/10.1016/j.autcon.2022.104707">https://doi.org/10.1016/j.autcon.2022.104707</a>
- [8] Liu W, Chen SE, Hauser E. Remote sensing for bridge health monitoring. In Atmospheric and Environmental Remote Sensing Data Processing and Utilization V: Readiness for GEOSS III, 2009; 7456, 100-109. SPIE. <a href="https://doi.org/10.1117/12.825528">https://doi.org/10.1117/12.825528</a>
- [9] Selvakumaran S, Plank S, Geiß C, Rossi C, Middleton C. Remote monitoring to predict bridge scour failure using Interferometric Synthetic Aperture Radar (InSAR) stacking techniques. International journal of applied earth observation and geoinformation, 2018; 73, 463-470. <a href="https://doi.org/10.1016/j.jag.2018.07.004">https://doi.org/10.1016/j.jag.2018.07.004</a>
- [10] Karimzadeh S, Ghasemi M, Matsuoka M, Yagi K, Zulfikar AC. A deep learning model for road damage detection after an earthquake based on synthetic aperture radar (SAR) and field datasets. IEEE Journal of Selected Topics in Applied Earth Observations and Remote Sensing, 2022; 15, 5753-5765. https://doi.org/10.1109/JSTARS.2022.3189875
- [11] Farneti E, Cavalagli N, Venanzi I, Salvatore W, Ubertini F. Residual service life prediction for bridges undergoing slow landslide-induced movements combining satellite radar interferometry and numerical collapse simulation. Engineering Structures, 2023; 293, 116628. <a href="https://doi.org/10.1016/j.engstruct.2023.116628">https://doi.org/10.1016/j.engstruct.2023.116628</a>
- [12] Boloorani AD, Darvishi M, Weng Q, Liu X. Post-war urban damage mapping using InSAR: the case of Mosul City in Iraq. ISPRS International Journal of Geo-Information, 2021; 10(3), 140. <a href="https://doi.org/10.3390/ijgi10030140">https://doi.org/10.3390/ijgi10030140</a>
- [13] Wen D, Huang X, Bovolo F, Li J, Ke X, Zhang A, Benediktsson JA. Change detection from very-high-spatial-resolution optical remote sensing images: Methods, applications, and future directions. IEEE Geoscience and Remote Sensing Magazine, 2021; 9(4), 68-101. https://doi.org/10.1109/MGRS.2021.3063465
- [14] Schlögl M, Widhalm B, Avian M. Comprehensive time-series analysis of bridge deformation using differential satellite radar interferometry based on Sentinel-1. ISPRS Journal of Photogrammetry and Remote Sensing, 2021; 172, 132-146. <a href="https://doi.org/10.1016/j.isprsjprs.2020.12.001">https://doi.org/10.1016/j.isprsjprs.2020.12.001</a>
- [15] Blikharskyy Y, Kopiika N, Khmil R, Selejdak J, Blikharskyy Z. Review of development and application of digital image correlation method for study of stress–strain state of RC Structures. Applied Sciences, 2022; 12(19), 10157. <a href="https://doi.org/10.3390/app121910157">https://doi.org/10.3390/app121910157</a>
- [16] Xiong S, Deng Z, Zhang B, Wang C, Qin X, Li Q. Deformation Evaluation of the South-to-North Water Diversion Project (SNWDP) Central Route over Handan in Hebei, China, Based on Sentinel-1A, Radarsat-2, and TerraSAR-X Datasets. Remote Sensing, 2023; 15(14), 3516. https://doi.org/10.3390/rs15143516
- [17] Nikolakopoulos KG, Kyriou A, Koukouvelas IK, Tomaras N, Lyros E. UAV, GNSS, and InSAR Data Analyses for Landslide Monitoring in a Mountainous Village in Western Greece. Remote Sensing, 2023; 15(11), 2870. <a href="https://doi.org/10.3390/rs15112870">https://doi.org/10.3390/rs15112870</a>

- [18] Yoon H, Shin J, Spencer Jr B F. Structural displacement measurement using an unmanned aerial system. Computer-Aided Civil and Infrastructure Engineering, 2018; 33(3), 183-192. <a href="https://doi.org/10.1111/mice.12338">https://doi.org/10.1111/mice.12338</a>
- [19] Davila Delgado JM, Butler LJ, Gibbons N, Brilakis I, Elshafie MZ, Middleton C. Management of structural monitoring data of bridges using BIM. In Proceedings of the Institution of Civil Engineers-Bridge Engineering, 2017; 170(3), 204-218. <a href="https://doi.org/10.1680/jbren.16.00013">https://doi.org/10.1680/jbren.16.00013</a>
- [20] Markogiannaki O, Chen F, Xu H, Mitoulis SA, Parcharidis I. Monitoring of a landmark bridge using SAR Interferometry coupled with engineering data and forensics. International Journal of Remote Sensing, 2022; 43(1):95-119. https://doi.org/10.1080/01431161.2021.2003468
- [21] Giordano PF, Turksezer ZI, Previtali M, Limongelli MP. Damage detection on a historic iron bridge using satellite DInSAR data. Structural Health Monitoring, 2022; 21(5), 2291-2311. https://doi.org/10.1177/14759217211054350
- [22] Peduto D, Giangreco C, Venmans AA. Differential settlements affecting transition zones between bridges and road embankments on soft soils: Numerical analysis of maintenance scenarios by multi-source monitoring data assimilation. Transportation Geotechnics, 2020; 24, 100369. https://doi.org/10.1016/j.trgeo.2020.100369
- [23] Alexander QG, Hoskere V, Narazaki Y, Maxwell A, Spencer Jr BF. Fusion of thermal and RGB images for automated deep learning based crack detection in civil infrastructure. AI in Civil Engineering, 2022; 1(1), 3. <a href="https://doi.org/10.1007/s43503-022-00002-y">https://doi.org/10.1007/s43503-022-00002-y</a>
- [24] Kim H, Sim SH, Spencer BF. Automated concrete crack evaluation using stereo vision with two different focal lengths. Automation in Construction, 2022; 135, 104136. <a href="https://doi.org/10.1016/j.autcon.2022.104136">https://doi.org/10.1016/j.autcon.2022.104136</a>
- [25] Terrados-Cristos M, Ortega-Fernández F, Díaz-Piloneta M, Montequín VR, González JG. Potential Structural Damage Characterization through Remote Sensing Data: A Nondestructive Experimental Case Study. Advances in Civil Engineering, 2022; 6557898. <a href="https://doi.org/10.1155/2022/6557898">https://doi.org/10.1155/2022/6557898</a>
- [26] Dong C Z, Catbas F N. A review of computer vision—based structural health monitoring at local and global levels. Structural Health Monitoring, 2021; 20(2), 692-743. https://doi.org/10.1177/1475921720935585
- [27] Dong C, Bas S, Catbas F N. Applications of computer vision-based structural monitoring on long-span bridges in Turkey. Sensors, 2023; 23(19), 8161. <a href="https://doi.org/10.3390/s23198161">https://doi.org/10.3390/s23198161</a>
- [28] Smail T, Abed M, Mebarki A, Lazecky M. Earthquake-induced landslide monitoring and survey by means of InSAR. Natural Hazards and Earth System Sciences, 2022; 22(5), 1609-1625. <a href="https://doi.org/10.5194/nhess-22-1609-2022">https://doi.org/10.5194/nhess-22-1609-2022</a>
- [29] Papadopoulos GA, Agalos A, Karavias A, Triantafyllou I, Parcharidis I, Lekkas E. Seismic and Geodetic Imaging (DInSAR) Investigation of the March 2021 Strong Earthquake Sequence in Thessaly, Central Greece. Geosciences. 2021; 11(8):311. https://doi.org/10.3390/geosciences11080311
- [30] Mavroulis S, Triantafyllou I, Karavias A, Gogou M, Katsetsiadou K-N, Lekkas E, Papadopoulos GA, Parcharidis I. Primary and Secondary Environmental Effects Triggered by the 30 October 2020, Mw = 7.0, Samos (Eastern Aegean Sea, Greece) Earthquake Based on Post-Event Field Surveys and InSAR Analysis. Applied Sciences. 2021; 11(7):3281. https://doi.org/10.3390/app11073281
- [31] Lekkas E, Mavroulis S, Gogou M, Papadopoulos GA, Triantafyllou I, Katsetsiadou KN, Kranis H, Skourtsos E, Carydis P, Voulgaris N, Papadimitriou P, Kapetanidis V, Karakonstantis A, Spingos I, Kouskouna V, Kassaras I, Kaviris G, Pavlou K, Sakkas V, Karatzetzou A, Evelpidou N, Karkani E, Kampolis I, Nomikou P, Lambridou D, Krassakis P, Foumelis M, Papazachos C, Karavias A, Bafi D, Gatsios T, Markogiannaki O, Parcharidis I, Ganas A,

- Tsironi V, Karasante I, Galanakis D, Kontodimos K, Sakellariou D, Theodoulidis N, Karakostas C, Lekidis V, Makra K, Margaris V, Morfidis K, Papaioannou C, Rovithis E, Salonikios T, Kourou A, Manousaki M, Thoma T, Karveleas N.(2020). The October 30, 2020 Mw 6.9 Samos (Greece) earthquake. Newsletter of Environmental, Disaster and Crises Management Strategies, 21, ISSN 2653-9454
- [32] Baek W K, Jung H S. Precise three-dimensional deformation retrieval in large and complex deformation areas via integration of offset-based unwrapping and improved multiple-aperture SAR interferometry: application to the 2016 Kumamoto earthquake. Engineering, 2020; 6(8), 927-935. <a href="https://doi.org/10.1016/j.eng.2020.06.012">https://doi.org/10.1016/j.eng.2020.06.012</a>
- [33] Bacastow TS, Bellafiore DJ. Redefining Geospatial Intelligence. Am. Intell. J. 2009; 27, 38–40. <a href="https://www.jstor.org/stable/44327109">https://www.jstor.org/stable/44327109</a>
- [34] Krassakis P, Karavias A, Nomikou P, Karantzalos K, Koukouzas N, Kazana S, Parcharidis I. Geospatial Intelligence and Machine Learning Technique for Urban Mapping in Coastal Regions of South Aegean Volcanic Arc Islands. Geomatics. 2022; 2(3):297-322. https://doi.org/10.3390/geomatics2030017
- [35] Markogiannaki O, Karavias A, Bafi D, Angelou D, Parcharidis I. A geospatial intelligence application to support post-disaster inspections based on local exposure information and on co-seismic DInSAR results: the case of the Durres (Albania) earthquake on November 26, 2019. Nat Hazards, 2020; 103, 3085–3100. https://doi.org/10.1007/s11069-020-04120-7
- [36] Krassakis P, Karavias A, Nomikou P, Karantzalos K, Koukouzas N, Kazana S, Parcharidis I. Geospatial Intelligence and Machine Learning Technique for Urban Mapping in Coastal Regions of South Aegean Volcanic Arc Islands. Geomatics. 2022; 2(3):297-322. <a href="https://doi.org/10.3390/geomatics2030017">https://doi.org/10.3390/geomatics2030017</a>
- [37] Krassakis P, Karavias A, Nomikou P, Karantzalos K, Koukouzas N, Athinelis I, Kazana S, Parcharidis I. Multi-Hazard Susceptibility Assessment Using the Analytical Hierarchy Process in Coastal Regions of South Aegean Volcanic Arc Islands. GeoHazards. 2023; 4(1):77-106. https://doi.org/10.3390/geohazards4010006
- [38] Krassakis P, Kazana S, Chen F, Koukouzas N, Parcharidis I, Lekkas E. Detecting subsidence spatial risk distribution of ground deformation induced by urban hidden streams. Geocarto International, 2019; 1–13. https://doi.org/10.1080/10106049.2019.1622601
- [39] Yun SH, Hudnut K, Owen S, Webb F, Simons M, Sacco P, Gurrola E, Manipon G, Liang C, Fielding E, Milillo P, Hua H, Colettaet A. Rapid damage mapping for the 2015 Mw 7.8 Gorkha earthquake using synthetic aperture radar data from COSMO-SkyMed and ALOS-2 satellites. Seismol Res Lett, 2015; 86(6):1549–1556. https://doi.org/10.1785/0220150152
- [40] Sharma RC, Tateishi R, Hara K, Thanh Nguyen H, Gharechelou S, Viet Nguyen L. Earthquake Damage Visualization (EDV) technique for the rapid detection of earthquake-induced damages using SAR data. Sensors, 2017; 17(2) <a href="https://doi.org/10.3390/s17020235">https://doi.org/10.3390/s17020235</a>
- [41] Preiss M, Gray DA, Stacy NJ. Detecting scene changes using synthetic aperture radar interferometry. IEEE Trans. Geosci. Remote Sens., 2006; 44(8), 2041-2054. <a href="https://doi.org/10.1109/TGRS.2006.872910">https://doi.org/10.1109/TGRS.2006.872910</a>.
- [42] Bouaraba A, Younsi A, Belhadj Aissa A, Acheroy M, Milisavljevic N, Closson D. Robust techniques for coherent change detection using COSMO-SkyMed SAR images, Progr. Electromagn. Res., 2012, 22, 219-232, <a href="https://doi.org/10.2528/PIERM11110707">https://doi.org/10.2528/PIERM11110707</a>.
- [43] ElGharbawi T, Zarzoura F. Damage detection using SAR coherence statistical analysis, application to Beirut, Lebanon. ISPRS Journal of Photogrammetry and Remote Sensing, 2021; 173, 1-9. <a href="https://doi.org/10.1016/j.isprsjprs.2021.01.001">https://doi.org/10.1016/j.isprsjprs.2021.01.001</a>

- [44] Spencer Jr B F, Hoskere V, Narazaki Y. Advances in computer vision-based civil infrastructure inspection and monitoring. Engineering, 2019; 5(2), 199-222. <a href="https://doi.org/10.1016/j.eng.2018.11.030">https://doi.org/10.1016/j.eng.2018.11.030</a>
- [45] Sacks R, Girolami M, Brilakis I. Building information modelling, artificial intelligence and construction tech. Developments in the Built Environment, 2020; 4, 100011. <a href="https://doi.org/10.1016/j.dibe.2020.100011">https://doi.org/10.1016/j.dibe.2020.100011</a>
- [46] Ren K, Zheng T, Qin Z, Liu X. Adversarial attacks and defenses in deep learning. Engineering, 2020; 6(3), 346-360. <a href="https://doi.org/10.1016/j.eng.2019.12.012">https://doi.org/10.1016/j.eng.2019.12.012</a>
- [47] Xing E P, Ho Q, Xie P, Wei D. Strategies and principles of distributed machine learning on big data. Engineering, 2016; 2(2), 179-195. <a href="https://doi.org/10.1016/J.ENG.2016.02.008">https://doi.org/10.1016/J.ENG.2016.02.008</a>
- [48] Narazaki Y, Hoskere V, Hoang T A., Fujino Y, Sakurai A, Spencer Jr B F. Vision-based automated bridge component recognition with high-level scene consistency. Computer-Aided Civil and Infrastructure Engineering, 2020; 35(5), 465-482. <a href="https://doi.org/10.1111/mice.12505">https://doi.org/10.1111/mice.12505</a>
- [49] LeCun Y, Bengio Y, Hinton G. Deep learning. Nature, 2015; 521(7553), 436-444. https://doi.org/10.1038/nature14539
- [50] Deng J, Singh A, Zhou Y, Lu Y, Lee VCS. Review on computer vision-based crack detection and quantification methodologies for civil structures. Construction and Building Materials, 2022; 356, 129238. https://doi.org/10.1016/j.conbuildmat.2022.129238
- [51] Pan Y, Braun A, Brilakis I, Borrmann A. Enriching geometric digital twins of buildings with small objects by fusing laser scanning and AI-based image recognition. Automation in Construction, 2022; 140, 104375. https://doi.org/10.1016/j.autcon.2022.104375
- [52] Zakaria M, Karaaslan E, Catbas F N. Advanced bridge visual inspection using real-time machine learning in edge devices. Advances in Bridge Engineering, 2022; 3(1), 1-18. https://doi.org/10.1186/s43251-022-00073-y
- [53] Vaswani A, Shazeer N, Parmar N, Uszkoreit J, Jones L, Gomez A N, Kaise Ł, Polosukhin I. Attention is all you need. Advances in neural information processing systems, 2017; 30.
- [54] Brown T, Mann B, Ryder, N, Subbiah M. Kaplan J. D, Dhariwal P, Pranav Shyam N, Sastry G, Askell A, Agarwal S, Herbert-Voss A, Krueger G, Henighan T, Child R, Ramesh A, Ziegler D, Wu J, Winter C, Hesse C, Chen C, Sigler E, Litwin M, Gray S, Chess B, Clark J, Berner C, McCandlish S, Radford A, Sutskever I, Amodei D. Language models are few-shot learners. Advances in neural information processing systems, 2020; 33, 1877-1901.
- [55] Drobnyi V, Li S, Brilakis I. Deep-learning guided structural object detection in large-scale, occluded indoor point cloud datasets. 2023 European Conference on Computing in Construction. Heraklion, Crete, Greece. July 10-12, 2023.
- [56] Du F, Jiao S, Chu K. Application research of bridge damage detection based on the improved lightweight convolutional neural network model. Appl. Sci. 2022; 12, 6225. https://doi.org/10.3390/app12126225
- [57] Hou F, Lei W, Li S, Xi J, Xu M, Luo J. Improved Mask R-CNN with distance guided intersection over union for GPR signature detection and segmentation. Automation in Construction, 2021; 121, 103414. <a href="https://doi.org/10.1016/j.autcon.2020.103414">https://doi.org/10.1016/j.autcon.2020.103414</a>
- [58] Zhang Y, Yuen K-V. Review of artificial intelligence-based bridge damage detection. Advances in Mechanical Engineering, 2022; 14(9). https://doi.org/10.1177/16878132221122770.

- [59] Mission ends for Copernicus Sentinel-1B satellite. Available at: https://www.esa.int/Applications/Observing\_the\_Earth/Copernicus/Sentinel-1/Mission ends for Copernicus Sentinel-1B satellite [accessed 15 September 2023].
- [60] Torres R, Snoeij P, Geudtner D, Bibby D, Davidson M, Attema E, Potin P, Rommen BO, Floury N, Brown M, Traver IN, Deghaye P, Duesmann B, Rosich B, Miranda N, Bruno C, L'Abbate M, Croci R, Pietropaolo A, Huchler M, Rostan F, GMES Sentinel-1 mission. Remote Sens. Environ., 2012; 120, 9–24. <a href="https://doi.org/10.1016/j.rse.2011.05.028">https://doi.org/10.1016/j.rse.2011.05.028</a>.
- [61] OpenStreetMap. Available online: https://www.openstreetmap.org/#map=9/36.6904/25.0516 [accessed on 19 September 2023].
- [62] Online source Damage In UA https://damaged.in.ua/about [accessed 15 October 2023]
- [63] Online source: The Eyes on Russia. The Centre for Information Resilience (CIR). https://eyesonrussia.org/about ure%2CFood+and+agriculture&dateRange=1644789600000%2C1695675600000&onlyEventsMapFrame=false
- ure%2CFood+and+agriculture&dateRange=1644789600000%2C1695675600000&onlyEventsMapFrame=talse [accessed 3 October 2023]
- [64] Online source: UADamage https://www.uadamage.com/map?h=MTIsMzguMDAxNjYsNDguNTkwNTU= [accessed 3 October 2023]
- [65] USGS EROS Archive—Digital Elevation—Shuttle Radar Topography Mission (SRTM) 1 Arc-Second Global. U.S. Geological Survey. Available online: https://www.usgs.gov/centers/eros/science/usgs-eros-archive-digital-elevation-shuttle-radar-topography-mission-srtm-1 [accessed 3 September 2023].
- [66] Closson D, Milisavljevic N. InSAR Coherence and Intensity Changes Detection. Mine Action-The Research Experience of the Royal Military Academy of Belgium, 2017; 292. <a href="https://doi.org/10.5772/65779">https://doi.org/10.5772/65779</a>
- [67] Stramondo S, Bignami C, Chini M, Pierdicca N, Tertulliani A. Satellite radar and optical remote sensing for earthquake damage detection: results from different case studies. International Journal of Remote Sensing, 2006; 27(20), 4433-4447. https://doi.org/10.1080/01431160600675895
- [68] Jung J, Yun S-H. Evaluation of Coherent and Incoherent Landslide Detection Methods Based on Synthetic Aperture Radar for Rapid Response: A Case Study for the 2018 Hokkaido Landslides. Remote Sensing. 2020; 12(2):265. <a href="https://doi.org/10.3390/rs12020265">https://doi.org/10.3390/rs12020265</a>
- [69] Kirillov A, Mintun E, Ravi N, Mao H, Rolland C, Gustafson L, Xiao T, Whitehead S, Berg AC, Lo WY, Dollár P, Girshick R Segment anything, 2023; arXiv preprint arXiv:2304.02643. https://doi.org/10.48550/arXiv.2304.02643
- [70] Chen K, Liu C, Chen H, Zhang H, Li W, Zou Z, Shi Z. RSPrompter: Learning to prompt for remote sensing instance segmentation based on visual foundation model. arXiv:2306.16269v2, 2023; https://doi.org/10.48550/arXiv.2306.16269
- [71] Liu S, Zeng Z, Ren T, Li F, Zhang H, Jie Y, Li C, Yang J, Su H, Zhu J, Zhang L. Grounding DINO: Marrying DINO with Grounded Pre-Training for Open-Set Object Detection. arXiv:2303.05499, 2023; https://doi.org/10.48550/arXiv.2303.05499
- [72] Li L, Zhang P, Zhang H, Yang J, Li C, Zhong Y, Wang L, Yuan L, Zhang L, Hwang J, Chang KW, Gao, J. Grounded Language-Image Pre-training. Proceedings of the IEEE/CVF Conference on Computer Vision and Pattern Recognition (CVPR), 2022; 10965-10975. https://doi.org/10.48550/arXiv.2112.03857

- [73] Radford A, Kim J, Hallacy C, Ramesh A, Goh G, Agarwal S, Sastry G, Askell A, Mishkin P, Clark J, Krueger G, Sutskever I. Learning Transferable Visual Models From Natural Language Supervision. Proceedings of the 38th International Conference on Machine Learning, PMLR, 2021; 139:8748-8763, <a href="https://doi.org/10.48550/arXiv.2103.00020">https://doi.org/10.48550/arXiv.2103.00020</a>
- [74] Narazaki Y, Hoskere V, Yoshida K, Spencer B, Fujino Y. Synthetic environments for vision-based structural condition assessment of Japanese high-speed railway viaducts. Mechanical Systems and Signal Processing, 2021; 160, 107850. <a href="https://doi.org/10.1016/j.ymssp.2021.107850">https://doi.org/10.1016/j.ymssp.2021.107850</a>
- [75] Bach Khoa Ho Chi Minh University. Crack detection using instance segmentation in yolov8 dataset (<a href="https://universe.roboflow.com/bach-khoa-ho-chi-minh-university-fyr43/crack-detection-using-instance-segmentation-in-yolov8">https://universe.roboflow.com/bach-khoa-ho-chi-minh-university-fyr43/crack-detection-using-instance-segmentation-in-yolov8</a>) [accessed 15 December 2023]
- [76] Rombach R., Blattmann A., Lorenz D., Esser P., Ommer B. High-resolution image synthesis with latent diffusion models. Proceedings of the IEEE/CVF conference on computer vision and pattern recognition, 2022; 10684-10695.
- [77] Television news service. http://surl.li/lzmkl, [accessed 3 October 2023]
- [78] Daniel Rice. Ukrainian Bridges are Playing a Vital Role in Both the Defense and the Offense in the Ukrainian-Russian War https://smallwarsjournal.com/jrnl/art/ukrainian-bridges-are-playing-vital-role-both-defense-and-offense-ukrainian-russian-war [accessed 3 October 2023]
- [79] Maria Engqvist. 2022. A Railhead Too Far: The Strategic Role of Railroads during Russia's Invasion of Ukraine (https://www.foi.se/rest-api/report/FOI%20Memo%207954) [accessed 3 October 2023]
- [80] Online source: https://twitter.com/detresfa\_/status/1501413574497153024 [accessed 3 October 2023]
- [81] Online source: https://www.abc.net.au/news/2022-03-06/ukrainians-cross-under-destroyed-bridge-irpin/100886922 [accessed 3 October 2023]

# Tiered approach for rapid damage characterisation of infrastructure enabled by remote sensing and deep learning technologies

Nadiia Kopiika<sup>(a)</sup>, Andreas Karavias<sup>(b)</sup>, Pavlos Krassakis<sup>(b)</sup>, Zehao Ye<sup>(a)</sup>, Jelena Ninic<sup>(a)</sup>, Nataliya Shakhovska<sup>(e,c,d)</sup>, Nikolaos Koukouzas<sup>(b)</sup>, Sotirios Argyroudis<sup>(e,f)</sup>, Stergios-Aristoteles Mitoulis<sup>(a,f)</sup>

- (a) University of Birmingham, Edgbaston, Birmingham, B15 2TT, UK
- (b) Centre for Research and Technology Hellas (CERTH), 15125 Athens, Greece
- (c) Lviv National Polytechnic University, Stepana Bandery St, 12, L'viv, Lvivska oblast, 79000, Ukraine
- (d) University of Agriculture in Krakow, Podłużna 3, 30-239, Poland
- (e) Brunel University London, Kingston Lane, Uxbridge Middlesex, UB8 3PH, UK
- (f) MetaInfrastructure.org, London, UK

Corresponding author:

Stergios-Aristoteles Mitoulis, <u>S.A.Mitoulis@bham.ac.uk</u>

#### The File Includes:

1.	Technical Terms				
	1.1.	InSAR imagery in infrastructure assessment [1],[2]	2		
	1.2.	Deep learning techniques in infrastructure assessment	5		
	1.3.	The research-related terminology	9		
2.	Su	pplementary materials	10		
	Table S.1. Tentative list, coordinates, and types of structures in the area of interest				
	Illust	tration of different LKn and DL for damage detection of 17 bridges (asset level)	11		
Re	eferenc	ces	13		

# 1. Technical Terms

# 1.1. InSAR imagery in infrastructure assessment [1],[2]

Earth Observation (EO) technologies encompass a diverse array of sophisticated remote sensing techniques and tools devised to gather data about the Earth's surface and atmosphere. Deployed across various platforms like satellites, aircraft, or ground-based sensors, these technologies are instrumental in monitoring the Earth's dynamic processes, environmental shifts, and human activities. The collected images undergo processing and analysis to extract a wide range of information, catering to diverse applications and industries. EO technologies employ different types of sensors, including optical and thermal sensors, which monitor the energy received from the Earth due to the reflection and re-emission of solar energy by the Earth's surface or atmosphere. Operating within the visible and infrared wavelengths of the electromagnetic spectrum, these sensors play a crucial role in capturing valuable data. Radar sensors, operating in the lower part of the spectrum with longer wavelengths, send energy to Earth and monitor the energy received back from the Earth's surface or atmosphere. This capability enables monitoring in all weather and light conditions. Thus, EO technologies make substantial contributions to environmental monitoring, agriculture, disaster management, urban planning, and climate research. They play a vital role in comprehending and addressing global challenges by providing valuable data for informed decision-making.

Synthetic-Aperture Radar (SAR) is a radar technology that relies on the movement of its antenna to generate high-resolution images of Earth's surfaces and objects. This active sensor transmits microwave signals and captures the signals reflected, or backscattered, from the Earth's surface. In contrast to traditional radar systems with fixed antennas, SAR systems emulate a large antenna by either moving or synthesizing the radar beam. This technology achieves detailed images with high spatial resolution, enabling the identification of small-scale objects and features on the ground. An essential characteristic of SAR is its capability to operate in diverse weather conditions, such as rain and clouds, making it suitable for remote sensing across various environments. Notably, SAR is an active sensor that emits its own microwave signals, enabling day and night operations independently of sunlight. This distinguishes SAR from optical technology. SAR's proficiency in detecting changes in habitat, water and moisture levels, the impact of natural or human disturbances, and alterations in Earth's surfaces after extreme events adds to its versatility. Moreover, SAR signals can penetrate through vegetation, facilitating observations of the Earth's surface even in densely forested regions. The wavelength of the sensor determines the depth of penetration into the vegetation layer, with longer wavelengths achieving deeper penetration, particularly in forested areas.

In summary, SAR imagery from satellites like Sentinel-1 is invaluable for remote sensing applications, playing a crucial role in assessing infrastructure damages, such as those to bridges, during conflicts or natural disasters. The interferometric capabilities of SAR further contribute to detecting landscape changes and evaluating damages over time.

Synthetic Aperture Radar (SAR) Interferometry (InSAR) is an advanced remote sensing radar technique that leverages the phase difference between two or more synthetic aperture radar images to precisely measure surface deformation. This method relies on the interference patterns created by combining radar signals acquired from slightly different positions. InSAR is particularly adept in geodesy and remote sensing, enabling the monitoring of ground displacement and topographic changes over time. This geodetic method finds applications in geophysical monitoring of both natural and human-induced hazards, and it plays a crucial role in structural engineering, especially for monitoring subsidence and assessing structural stability. InSAR has the potential to measure millimeter-scale changes in deformation over varying time spans, ranging from days to years. Key applications of SAR Interferometry encompass monitoring subsidence, detecting shifts in the Earth's crust, assessing infrastructure deformation, and evaluating changes in land topography. InSAR has demonstrated its value across diverse fields such as geology, environmental monitoring, and infrastructure management, providing detailed insights into surface movements on a global scale.

In practical terms, during InSAR, radar waves emitted by a satellite or airborne platform interact with the Earth's surface and return as **backscattered signals**. The amount of radar energy reflected back to the radar antenna from the Earth's surface is defined by **the backscatter intensity**, being commonly represented as grayscale values in InSAR images. High backscatter intensity (at areas with brighter grayscale values) can be associated with surfaces that strongly reflect radar signals, such as buildings, rocks, or dense vegetation.

**Phase signals** in InSAR images represent the difference in the phase of radar waves between two or more radar acquisitions. By comparing the phase information of two signals between multiple acquisitions, InSAR detects changes in the distance travelled by the radar waves, enabling the identification of ground movements. Depending on the configuration, InSAR can map the topography of the surface or reveal motion and deformation over time.

Sentinel-1 coherence serves as an indicator of the constancy or steadiness of the phase difference between two Synthetic Aperture Radar (SAR) images acquired by the Sentinel-1 satellite over the same geographic area but at different time points. The coherence data is extracted from interferometric SAR (InSAR) data, a process that involves merging multiple radar images to generate an interferogram. The interferogram visually illustrates the phase difference between two radar images through fringes, where each fringe corresponds to a specific phase change. Coherence, thus, is a parameter that quantifies the stability of the phase difference between two radar images. It ranges from 0 to 1, with 1 indicating perfect coherence (high stability) and 0 indicating no coherence (low stability). Elevated coherence suggests minimal or no change between the two acquisition instances. Coherence can fluctuate over time due to factors such as alterations in vegetation, atmospheric conditions, or ground movement. The monitoring of coherence changes aids in comprehending the stability of the observed area. Sentinel-1 coherence is valuable for monitoring various Earth surface phenomena, including deformation analysis, land subsidence, vegetation monitoring, and infrastructure stability. High coherence is desirable for accurate interpretation of ground movement. The coherence  $(\gamma)$ , as the complex correlation coefficient between two SAR scenes  $u_1$  and  $u_2$ , is estimated as:

$$\gamma = \frac{E\left[u_{1}u_{2}^{*}\right]}{\sqrt{E\left[\left|u_{1}\right|^{2}\right]}\sqrt{E\left[\left|u_{2}\right|^{2}\right]}}$$

where  $E\{\}$  represents the mathematical expectation and \* is the complex conjugate operator. Coherence is a crucial metric for interpreting InSAR data, offering insights into the stability of the observed area over time. It is widely used in Earth observation applications for environmental monitoring, geohazards assessment, and infrastructure management.

Coherent Change Detection (CCD) technique is a method employed in remote sensing, particularly in the analysis of Synthetic Aperture Radar (SAR) imagery, to identify and assess significant changes within a specific area over two or more radar acquisitions. In the CCD estimation process, multiple high-resolution satellite radar images of a geographic area taken at different times are compared to detect and quantify changes. A distinctive aspect of CCD lies in its ability to leverage the phase information of SAR images to identify alterations in the scene. Unlike methods focused on topographic information, CCD emphasizes phase differences resulting from temporal changes in the scene.

The approach involves comparing Sentinel-1 coherence products across two temporal periods. An algorithm is applied to this comparison, considering both the geographic area and mission parameters. High coherence values are anticipated when the first coherence product is derived from a pair of images within the closest dataset. Conversely, if the second image is obtained after a specific event, the decorrelation in phase is revealed through coherence change detection (CCD).

CCD is particularly beneficial in applications where monitoring subtle yet coherent changes in the landscape is essential. It is extensively utilized for detecting infrastructure deformations, land subsidence, and other ground movements. This technique serves as a robust tool for change detection in areas where traditional optical imagery may be limited, such as regions with persistent cloud cover or during nighttime.

The Sentinel-1 Single Look Complex (SLC) products represent sophisticated synthetic aperture radar (SAR) data provided by the Sentinel-1 satellite mission, offering in-depth insights into the Earth's surface. The designation "Single Look Complex" pertains to a specific SAR data format, wherein each pixel in the image corresponds to a single radar echo. The processing of SLC products ensures a single look in each dimension, utilizing the full available signal bandwidth and geo-referencing the imagery using orbit and attitude data from the satellite. SLC images are characterized by the highest fidelity among all SAR image products, as they are only one step removed from the original collected RADAR data. They retain the original sensor measurements, devoid of interpolation artifacts or projection issues. Although the default SLC product reduces the dynamic range of complex numbers for manageable image sizes, it remains a valuable resource for a variety of applications. The amplitude information in SLC products reflects the strength of the radar signal reflected from

the Earth's surface, while the phase information indicates the position of the radar wave during interaction with the surface. SLC data finds utility in interferometric applications, facilitating the generation of interferograms for InSAR analysis. Sentinel-1 SLC products prove beneficial for diverse applications, encompassing the monitoring of ground movements, subsidence, land deformation, changes in vegetation, disaster management, infrastructure monitoring, and environmental studies. While SLC products are considered the optimal source for SAR image analysis, their complex nature necessitates specialized software and expertise. Automated processing and advanced exploitation, particularly in interferometric applications, are common uses for SLC images. Orthorectification of the SLC product can be achieved using specialized SAR software tools such as the **European Space Agency (ESA) Sentinel Application Platform (SNAP).** 

The Sentinel Application Platform (SNAP) is a specialized software tool developed by the European Space Agency (ESA), (in collaboration with Brockmann Consult, SkyWatch, and C-S). Its primary purpose is the processing and analysis of data sourced from the Sentinel satellites, presenting a comprehensive and userfriendly platform tailored for various remote sensing data, with a specific emphasis on the Sentinel missions such as Sentinel-1 and Sentinel-2. In the realm of Synthetic Aperture Radar (SAR) data, SNAP provides tools for interferometric processing, facilitating the creation of interferograms crucial for applications like interferometric SAR (InSAR) analysis. SNAP offers a user-friendly interface for visualizing and exploring remote sensing data through interactive maps and graphical displays, fostering a deeper comprehension of the acquired information. The software ensures swift image display and navigation, allowing users to add and manipulate new overlays. It encompasses a suite of tools for processing remote sensing data, encompassing tasks like calibration, filtering, and correction techniques. SNAP supports the generation of various products, including Level-1, Level-2, and Level-3 data. One distinctive feature of SNAP is its incorporation of a graph processing framework, empowering users to create custom processing chains and execute intricate processing workflows. This modular and adaptable approach significantly enhances the customization and automation of data processing tasks. As a pivotal tool in the analysis of Sentinel satellite data, SNAP empowers researchers, scientists, and professionals to extract meaningful insights from Earth observation data, facilitating applications such as environmental monitoring, land use analysis, and disaster management.

Interferometric Wide Swath (IW) Synthetic Aperture Radar (SAR) images are the type of SAR data acquired by the Sentinel-1 satellite mission, specifically from its Interferometric Wide Swath mode. In this operational mode, SAR technology is used to capture images with a wide coverage, enabling the observation of large areas on the Earth's surface. A single Sentinel-1 satellite has the potential to map global landmasses in the Interferometric Wide Swath mode approximately every 12 days, either in a single pass (ascending or descending). Thus, the two-satellite constellation provides a precise 6-day repeat cycle at the equator. These images are well-suited for interferometric applications, including Interferometric SAR (InSAR) analysis. The combination of interferometric capabilities and extensive spatial coverage renders IW SAR images from the Sentinel-1 mission particularly valuable for tasks such as monitoring ground displacements, investigating land deformation, and evaluating changes in vegetation cover on a regional scale.

The primary data acquisition **Interferometric Wide (IW) swath mode** meets the majority of service requirements. This mode collects data with a 250 km swath at a spatial resolution of  $5\times20$  m (single look). The IW mode employs **Terrain Observation with Progressive Scans SAR (TOPSAR)**, capturing three subswaths. The **TOPSAR technique**, a form of ScanSAR imaging, involves acquiring data in bursts by cyclically switching the antenna beam between multiple adjacent sub-swaths. TOPSAR acquisitions offer the advantage of large swath widths and improved radiometric performance, minimizing the scalloping effect, and ensuring consistent image quality throughout the entire swath.

The TOPSAR-split operator is used for the processing and coherent combination of data obtained from different sub-swaths. In the TOPSAR mode, data is collected in bursts by cyclically switching the antenna beam between multiple adjacent sub-swaths. The split operator manages the processing of received signals from different sub-swaths by separating them during burst acquisition and then coherently recombining them during data processing. This is crucial to ensure that the resulting Synthetic Aperture Radar (SAR) image maintains coherence and quality across the entire swath.

The TOPSAR-deburst operator is employed to handle and process bursts of data coherently. Its primary function is to eliminate the effects of burst transitions and ensure the seamless combination of data from different sub-swaths. The TOPSAR deburst operator helps eliminating discontinuities and artifacts that may arise due to the cyclic switching of the antenna beam. By coherently combining burst data, the deburst operator contributes to the production of a high-quality and coherent SAR image over the entire swath.

The TOPSAR-multilook operator is employed to enhance the signal-to-noise ratio and reduce speckle in SAR images. Speckle is a granular noise that can impact the quality of the image in SAR imaging. The multilooking process involves averaging multiple looks or samples of the radar data within each resolution cell, effectively smoothing out the speckle and enhancing image quality. It helps mitigate the impact of speckle, providing a clearer and more visually interpretable SAR image and contributes to the overall radiometric performance of the image.

The Shuttle Radar Topography Mission (SRTM-1), conducted by NASA in February 2000, aimed to enhance the precision and resolution of global elevation data. Its primary goal was to generate a comprehensive and high-resolution Digital Elevation Model (DEM) of the Earth. Using the Space Shuttle Endeavour, the mission deployed a specialized radar system, specifically the Spaceborne Imaging Radar-C/X-Band Synthetic Aperture Radar (SIR-C/X-SAR), known for its ability to penetrate cloud cover and capture topographic details with high accuracy. SRTM-1 targeted global coverage, encompassing elevation data for a significant portion of the Earth's land surface within the latitudinal range of 60 degrees north to 56 degrees south. The mission aimed to achieve a horizontal resolution of approximately 30 meters, providing intricate elevation details for diverse applications. The resulting SRTM-1 data has found widespread use in scientific research, environmental monitoring, terrain modelling, geological studies, and various applications requiring precise topographic information. This mission has substantially contributed to the availability of high-quality elevation data, emerging as a valuable resource for researchers and professionals in Earth sciences and geospatial fields. The Digital Elevation Model (DEM) produced by the Shuttle Radar Topography Mission (SRTM-1) provided a detailed representation of the Earth's topography, offering elevation information at a resolution of about 30 meters. This global dataset has been extensively employed in applications such as terrain modelling, environmental monitoring, hydrological analysis, and geospatial research.

# 1.2. Deep learning techniques in infrastructure assessment

**Artificial intelligence (AI)** refers to the development of computer systems or software that can perform tasks that typically require human intelligence. These tasks include learning, reasoning, problem-solving, understanding natural language, perception, and even the ability to interact with the environment. The ultimate goal of AI is to create machines that can replicate or simulate human cognitive functions.

AI technologies can be categorized into various subfields, such as machine learning, natural language processing, computer vision, robotics, and expert systems. Machine learning, a subset of AI, involves training algorithms on data to recognize patterns and make decisions without explicit programming.

The applications of AI are diverse and can be found in areas such as healthcare, finance, education, manufacturing, entertainment, and more. The field continues to advance rapidly, with ongoing research and development seeking to improve AI systems' capabilities, efficiency, and ethical considerations.

Machine learning (ML) is a cutting-edge programming technique used to automate the construction of analytical models and enable applications to perform specified tasks more efficiently without being explicitly programmed. Machine learning allows the system to automatically learn and increase its accuracy in task performance through experience. Machine learning is an application of artificial intelligence that simulates the learning process by establishing a predictive model, analysing its output given specified parameters, and progressively updating the model to increase its accuracy. ML is focused on the development of algorithms and statistical models that enable computers to perform tasks without explicit programming. The core idea behind machine learning is to allow machines to learn from data and improve their performance over time without being explicitly programmed for a particular task.

Machine learning models require a set of data for **training.** This data includes examples or instances of the task that the model is supposed to learn. The more diverse and representative the training data, the better the model's generalization. The machine learning model is trained on a subset of the data, and its performance is

evaluated on another subset (testing data) to ensure that it generalizes well to new, unseen examples. The model's performance is assessed based on metrics relevant to the specific task (e.g., accuracy, precision, recall). If the performance is not satisfactory, the model may be adjusted, retrained, or fine-tuned.

**Features** are the variables or characteristics of the data that the model uses to make predictions or decisions. The selection of relevant features is crucial for the model's performance.

Machine learning algorithms are the mathematical and computational procedures used to train models based on the provided data. These algorithms can be categorized into various types, such as supervised learning, unsupervised learning, and reinforcement learning.

Machine learning is applied in various domains, including image and speech recognition, natural language processing, recommendation systems, autonomous vehicles, fraud detection, and many others. As technology and research progress, machine learning continues to play a crucial role in advancing the capabilities of artificial intelligence.

**Deep learning (DL)** is a subfield of machine learning that focuses on the use of artificial neural networks to enable machines to learn and make decisions. It is called "deep" learning because it involves neural networks with many layers (deep neural networks). These networks are capable of learning intricate patterns and representations from vast amounts of data, allowing them to perform complex tasks. Deep learning models are trained through a process called **backpropagation**. During training, the model makes predictions, and the error or the difference between the predicted output and the actual output is calculated. The error is then used to adjust the model's weights through the layers to minimize the difference in subsequent predictions. Deep learning applications process information using artificial neural networks, highly connective computer systems that were designed to mimic the biological structure of the human brain. Deep learning models often benefit from **transfer learning**, where a pre-trained model on a large dataset is fine-tuned for a specific task with a smaller dataset. This approach leverages the knowledge gained from the pre-training process.

Deep learning has achieved remarkable success in various applications, including image and speech recognition, natural language processing, autonomous vehicles, healthcare, and more. Its ability to automatically learn complex representations from data has contributed to its widespread adoption in solving challenging real-world problems.

**Neural Network approach**. At the core of deep learning are artificial neural networks, which are computational models inspired by the structure and functioning of the human brain. A neural network is composed of layers of interconnected nodes (neurons), each layer processing information and passing it on to the next layer. Connections between nodes are represented by weights (and bias), which the network learns during training. Learning occurs through a process called backpropagation, where the network adjusts its weights based on the error between predicted and actual outputs. Deep learning involves using neural networks with multiple hidden layers, allowing them to learn hierarchical representations of data. Each layer captures different features or abstractions, enabling the network to understand increasingly complex patterns. Neural networks can be applied to various tasks, including image recognition, natural language processing, speech recognition, and more. Depending on the specific task and data characteristics, different **neural network architectures** (e.g., Convolutional Neural Networks, Recurrent Neural Networks) may be chosen to optimize performance.

Convolutional Neural Network (CNN) is a type of deep neural network designed specifically for tasks related to computer vision, image recognition, and image processing. CNNs have proven to be highly effective in capturing spatial hierarchies of features in images, making them well-suited for tasks such as object detection, image classification, and facial recognition. The architecture of a CNN is characterized by the use of convolutional layers, pooling layers, and fully connected layers. Convolutional Neural Networks have demonstrated remarkable performance in various computer vision tasks, and their architecture has been adapted and extended to address different challenges. Notable CNN architectures include LeNet, AlexNet, VGG, GoogLeNet (Inception), ResNet, and more, each with specific design choices to achieve state-of-the-art performance in different applications.

The **ImageNet dataset** is a large-scale image database designed for use in visual object recognition and image classification research. It played a crucial role in advancing the development of deep learning models, particularly **Convolutional Neural Networks (CNNs).** ImageNet contains millions of labelled images from a wide variety of categories, spanning objects, animals, scenes, and more. The dataset has over 1,000 object

categories, making it a comprehensive benchmark for evaluating the performance of image classification models. ImageNet Large Scale Visual Recognition Challenge (ILSVRC) is a well-known annual competition associated with this dataset, that tasks participants with developing models capable of accurately classifying objects in the ImageNet dataset. Participants are provided with a training set for model development and a test set for evaluation. Many deep learning architectures that gained prominence in the ImageNet challenges have become standard benchmarks for other computer vision tasks. For example, ResNet introduced the concept of residual learning, which has been widely adopted in various applications.

Computer Vision (CV) is a sector of artificial intelligence (AI), a multidisciplinary field, leveraging machine learning and deep learning to empower computers and systems in comprehending and making sense of visual information. It involves the development of algorithms, models, and systems that allow machines to gain insights from images or videos, process visual data, and make decisions based on visual input. The goal of computer vision is to endow computers with the ability to see, perceive, and interpret the visual world in a manner similar to human vision. CV aims to emulate the intricacies of human vision. With continuous progress in AI, this domain has not only achieved parity with human capabilities but has also exceeded them in certain CV tasks, particularly in areas like image classification, object detection, semantic segmentation, action recognition, etc.. Computer Vision continues to evolve with advancements in machine learning, deep learning, and sensor technologies, making it a critical field with a wide range of practical applications across various industries.

Automated vision-based structural inspection is the process of utilizing automated vision systems, including cameras, image processing algorithms, and remote sensing techniques, to inspect and analyse the structural integrity of buildings, bridges, or other infrastructures. This approach involves capturing images or videos and analysing them automatically, along with utilizing remote sensing data, to identify potential issues such as defects, damages, or anomalies. It offers a faster, more efficient, and potentially more accurate method compared to traditional manual inspection techniques.

Semantic segmentation algorithms are computer vision techniques used to classify each pixel in an image into predefined semantic categories, for solving one of the key tasks in the field of computer vision. These algorithms assign a single label to each pixel, indicating the category to which it belongs, but they do not differentiate between instances of the same class. This allows for a pixel-wise understanding of the scene, enabling applications such as scene understanding, object detection, and image segmentation. Semantic segmentation algorithms typically employ deep learning architectures to learn rich feature representations and accurately assign semantic labels to pixels in an image.

The method of transformer-based architecture refers to a deep learning approach that utilizes the transformer model, originally developed for natural language processing (NLP), and extends its application to computer vision tasks. Unlike traditional CNNs, which process images hierarchically, transformer-based architectures operate on the entire image as a sequence of tokens. This enables them to capture long-range dependencies and global context effectively. In computer vision, transformer-based architectures are employed for tasks such as image classification, object detection, and image generation. These architectures typically consist of multiple transformer layers that perform self-attention operations to compute relationships between different parts of the input image. Pre-training on large datasets using self-supervised learning techniques, followed by fine-tuning on specific tasks using supervised learning, is a common practice. Overall, transformer-based architectures offer competitive performance and flexibility in handling various types of visual data.

Large language models are advanced natural language processing (NLP) models that are trained on vast amounts of text data, possessing millions or even billions of parameters. These models leverage deep learning techniques, particularly transformer-based architectures, to capture intricate linguistic patterns and nuances. With their extensive size and complexity, large language models excel at tasks such as text generation, translation, summarization, and understanding, demonstrating human-like capabilities in processing, and producing natural language text.

Robust zero-shot and few-shot generalization capabilities refer to the model's ability to effectively handle tasks it hasn't encountered during training without extensive additional data. Zero-shot generalization means the model can perform adequately on entirely new tasks by extrapolating knowledge from related tasks, while

few-shot generalization indicates the model can learn from a minimal number of labelled examples for new tasks. These capabilities are crucial for real-world applications, where adapting to novel scenarios quickly and efficiently is essential.

The Bidirectional Feature Pyramid Network model is an advanced architecture utilized in object detection tasks within computer vision. It enhances the Feature Pyramid Network (FPN) by integrating bidirectional connections between adjacent feature maps, enabling effective fusion of low-level and high-level features. This adaptation, along with learnable weights, enhances the model's ability to represent objects of varying scales accurately, ultimately leading to improved performance and robustness in object detection across different datasets and scenarios.

**Intersection over Union (IoU) metric** is a measure frequently employed in computer vision tasks. It quantifies the degree of overlap between the predicted and ground truth bounding boxes or masks by calculating the ratio of their intersecting area to their combined area. A higher IOU score signifies better alignment between the predicted and actual bounding boxes or masks, with a maximum score of 1 indicating perfect overlap. This metric serves as a standard assessment tool for evaluating the precision of object localization/segmentation, aiding in the refinement and optimization of CV algorithms.

Pretrained YOLO (You Only Look Once) model refers to a CNN architecture that has been trained on a large dataset for object detection tasks using the YOLO framework. The YOLO model is a popular real-time object detection algorithm in computer vision. Unlike traditional approaches that require multiple passes through the network for object detection, YOLO processes the entire image in a single forward pass, enabling fast and efficient detection of objects. It divides the input image into a grid and predicts bounding boxes and class probabilities for objects directly from the grid cells. YOLO is known for its speed and accuracy, making it widely used in applications such as autonomous driving, surveillance, and image. It has become a representative series of algorithms. The pretrained YOLO model has already learned to recognize and localize objects in images across various classes, such as people, cars, animals, and more, by accurately predicting bounding boxes and class labels for objects present in an input image. Leveraging a pretrained YOLO model enables developers and researchers to fine-tune the model on specific datasets or tasks with minimal additional training, reducing the time and computational resources needed to develop object detection systems for new applications.

Mask Region-based Convolutional Neural Network (R-CNN) architecture, or Mask R-CNN, is an advanced deep learning architecture designed for instance segmentation tasks in computer vision. It extends the Faster R-CNN framework by incorporating an additional branch for predicting segmentation masks alongside object detection, enabling pixel-level accuracy in delineating object boundaries. This allows Mask R-CNN to perform precise instance segmentation, distinguishing between different instances of the same class within an image, and has demonstrated state-of-the-art performance in various tasks such as object detection and key point detection.

**Segment Anything Model (SAM)** is a new AI model from Meta AI that can "cut out" any object, in any image, with some simple prompts. It is a promptable segmentation system with zero-shot generalization to unfamiliar objects and images, without the need for additional training. It is pre-trained on the largest-ever dataset (SA-1B) generated by a data engine, comprising over one billion masks in 11 million images, which is 400 times larger than the existing datasets. SAM aims to develop a robust foundation model for segmentation, designed as a prompt model without active recognition ability.

Query-based learnable prompt SAM algorithm is a method used for self-generating prompt for SAM, so as to make SAM can carry out automatically. It employs a learnable prompt mechanism to generate adaptable and informative appropriate prompts for SAM. The query-based prompter is primarily composed of a Transformer encoder and decoder. Overall, it transforms the preset learnable query into the prompt embedding for SAM and corresponding semantic categories.

**Stable Diffusion for Occlusion Repair** refers to a method used in image processing and computer vision for inpainting, which is the process of filling in missing or damaged parts of an image. Stable diffusion techniques aim to efficiently propagate information from known regions of the image to reconstruct the missing parts while preserving important visual characteristics such as texture, edges, and colour consistency. These methods typically involve iterative algorithms that diffuse information across the image domain while controlling the

diffusion process to ensure stability and coherence in the inpainted result. Stable diffusion is essential for applications like image restoration, digital image editing, and medical image analysis where accurate reconstruction of missing information is critical.

Contrastive Language-Image Pre-Training (CLIP) is a methodology in artificial intelligence and machine learning that focuses on training models to understand the relationship between language and images through contrastive learning. In CLIP, a large-scale dataset containing pairs of images and corresponding text descriptions is used to train a neural network model. The dataset is collected from the Internet by OpenAI. The model is trained to associate similar images and text representations while distinguishing dissimilar pairs. By learning to understand the relationship between images and their textual descriptions, CLIP enables the model to perform various tasks, including image classification, object detection, and image generation, based on natural language queries or descriptions. This approach allows CLIP to achieve state-of-the-art performance across a wide range of vision and language tasks without task-specific training, making it a versatile and powerful tool in the field of artificial intelligence.

Grounded Language-Image Pre-training (GLIP) is a multimodal language-image model. Similar to CLIP, it performs contrastive pretraining to learn semantically rich representations and align them across modalities. While CLIP learns these representations at the image level, meaning a single sentence describes the entire image, GLIP aims to extend this approach to object-level representations, meaning a single sentence may correspond to multiple objects in the image. The task of identifying the correspondence between individual tokens in textual prompts and objects or regions in the image is called phrase grounding. Hence, the term "grounded" is used in GLIP. Therefore, the objectives of GLIP is unified phrase grounding and object detection for large-scale pretraining.

**Tokaido dataset** is a publicly available synthetic dataset that firstly published at the 2nd International Competition for Structural Health Monitoring (IC-SHM, 2021), consisting of 1,750 railway viaducts with random geometry realized by the actual design procedure. In the dataset, random damages, including concrete cracks and exposed rebar, could present on the viaduct columns. For the structural component segmentation task, there are 8,648 images with seven classed of components: non-bridge, slab, beam, column, non-structural, rail, and sleeper. For the damage segmentation tasks, the dataset has 7,990 real scene images and 2,700 pure texture images with three classes: non-damage, concrete damage, and exposed rebar.

**Grounding DINO** is an open-set object detector, by marrying Transformer-based detector DINO (a form of knowledge distillation with no labels) with grounded pre-training, which can detect arbitrary objects with human inputs such as category names or referring expressions.

**Grounded-SAM** is to combine Grounding DINO and SAM which aims to detect and segment anything with text inputs.

# 1.3. The research-related terminology

**Human-induced hazards/Anthropogenic disasters (in this research)** are catastrophic events caused or significantly influenced by human activities, causing potential threats or dangers to the environment, society, or infrastructure. This study is focused on the particular group of such accidents, integrating destructions caused by terrorist attacks, military activities and hostilities at conflict-prone territories. These hazards can have severe consequences for human populations, infrastructure, and the environment, encompassing a range of threats, and their impacts can be both immediate and long-lasting. Addressing war-induced hazards requires comprehensive efforts, including conflict prevention, peacebuilding, humanitarian assistance, and post-conflict reconstruction.

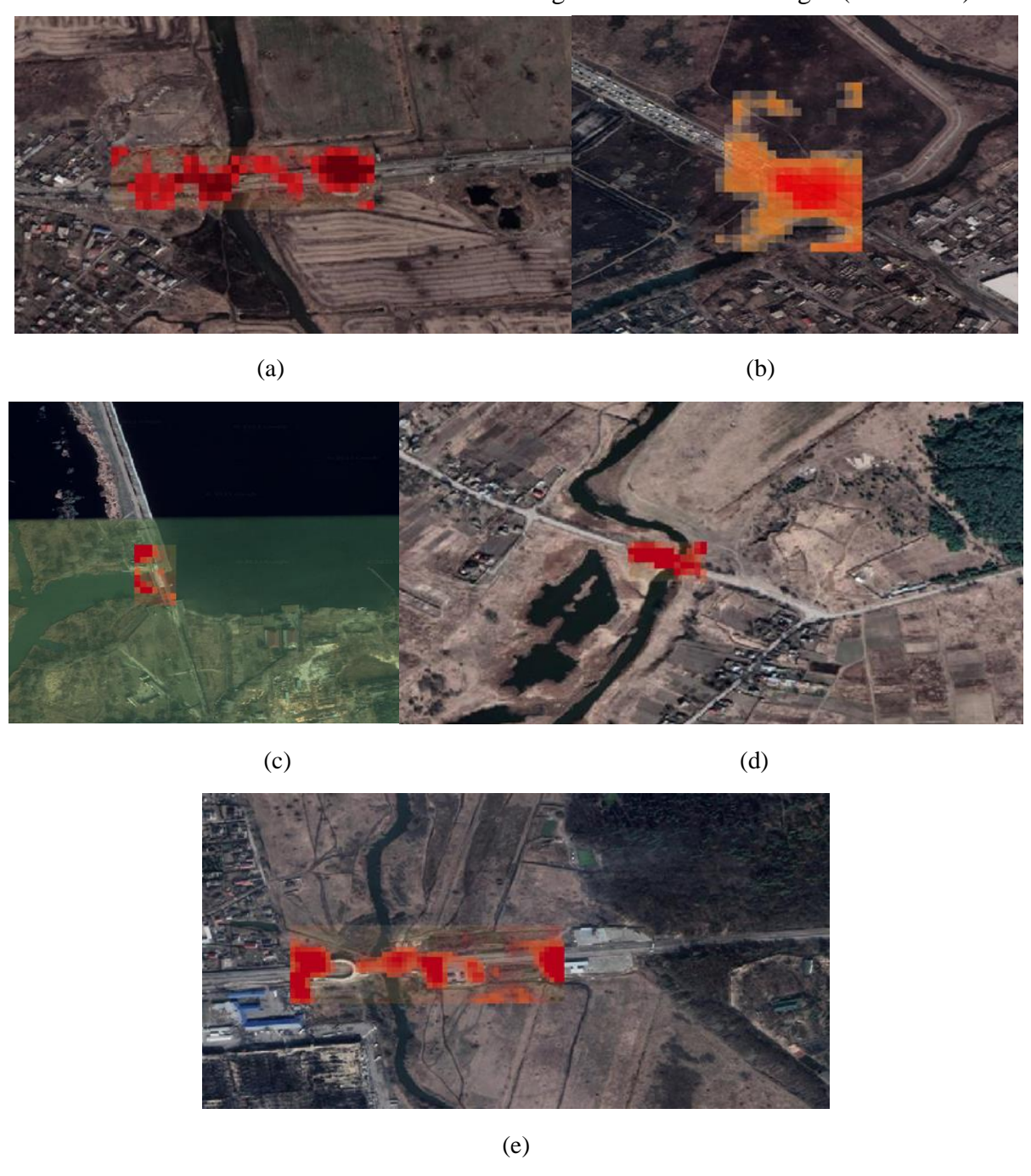
The Level of Knowledge (LKn) (in this research): the proposed parameter for estimation of reliability of damage detection at asset level. As the study is focused on sources of data, freely accessible during the hostilities, the utilized Sentinel-1 imaginary reveal certain limitations. Thus, all the assets were classified, according two three Levels of Knowledge: low (LKn<sub>L</sub>), medium (LKn<sub>M</sub>), and high (LKn<sub>H</sub>), identifying the applicability of the approach.

The Damage Level (DL) (in this research): the proposed grouping of assets according to change of coherence between the pairs of images from two datasets Thus, structures were classified in groups of :  $DL_L$  (low),  $DL_M$  (moderate),  $DL_H$  (high).

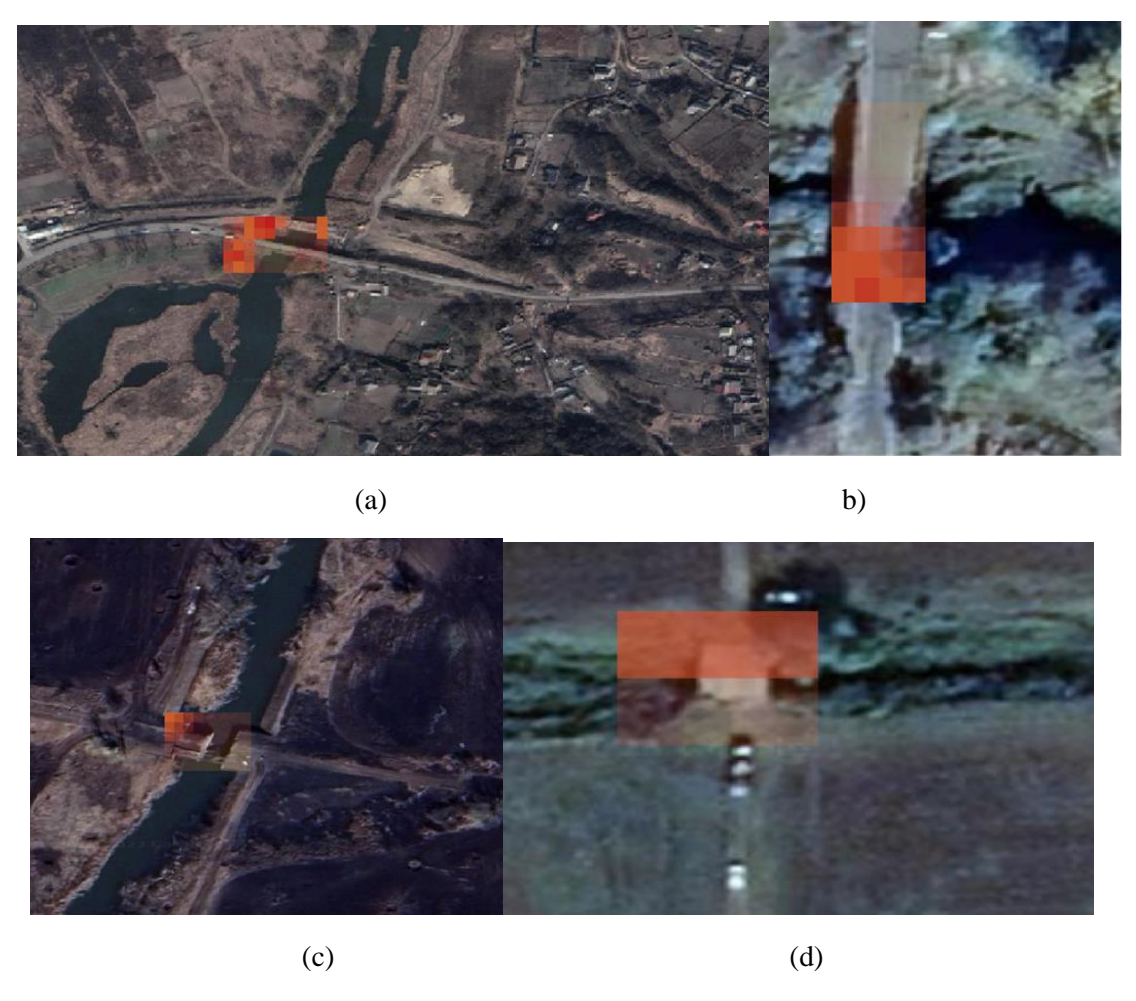
# 2. Supplementary materials

**Table S.1.** Tentative list, coordinates, and types of structures in the area of interest

Asset ID	Length/Width (m)	Type	Lon, Lat		
1 90/24		Bridge	50°29'29.680" N	50°29'27.063" N	
			30°15'28.934" E 50°33'12.613" N	30°15'33.716" E 50°33'12.017" N	
2	140/27	Bridge	30°17'8.608" E	30°17'2.319" E	
			50°23'28.229" N	50°23'28.590" N	
3	85/10	Bridge	30°13'5.070" E	30°13'3.212" E	
			50°39'51.805" N	50°39'52.292" N	
4	35/8	Bridge	30°16'51.514" E	30°16'50.869" E	
			50°11'50.698" N	50°11'52.097" N	
5	36/9.9	Bridge	29°50'10.434" E	29°50'10.523" E	
			50°44'36.703" N	50°44'40.140" N	
6	155/10	Bridge +Dam	30°22'8.149" E	"30°22'6.879" E	
			50°36'39.687" N	50°36'39.872" N	
7	41/9	Bridge	30°16'50.213" E	30°16'49.264" E	
			50°42'44.851" N	50°42'49.559" N	
8	60/19	Bridge	30°20'22.571" E	30B°20'19.429"E	
			50°15'0.959" N	50°15'1.344" N	
9	87/11	Bridge	29°59'59.243 " E	29°59'58.128" E	
		Bridge +	50°18'11.437" N	50°18'12.102" N	
10	34/4.5	Embankment	30°4'49.621" E	30°4'49.269" E	
		Linoankinent	50°27'25.228" N	50°27'24.733" N	
11	25/4.2	Bridge+Weir	30°14'12.463" E	30°14'13.572" E	
		Bridge +	50°16'20.038" N	50°16'20.753" N	
12	23/7	Embankment	30°2'32.858" E	30°2'32.248" E	
	24/2 25/3	Bridge Bridge	50°22'49.958" N	50°22'50.667" N	
13			30°11'12.009" E	30°11'12.114" E	
			50°17'16.262" N	50°17'16.219" N	
14			30°3'31.742" E	30°3'33.732" E	
			50°12'52.507" N	50°12'52.984" N	
15	22/8	Bridge	29°52'49.863" E	29°52'49.809" E	
	15/4		50°12'26.815" N	50°12'27.351" N	
16	15/4	Bridge	29°57'31.024" E	29°57'31.782" E	
	150/00		50°26'50.775" N	50°26'50.593" N	
17	173/30	Bridge	30°14'7.284" E	30°14'4.834" E	
			50°11'50.983" N	50°11'50.119" N	
18		-	29°50'13.511" E	29°50'13.293" E	
10	-		50°20'4.443" N	50°20'4.432" N	
19		-	30°8'49.324" E	30°8'48.161" E	
20			50°23'49.212" N	50°23'49.561" N	
20	-	-	30°13'0.984"E	30°13'1.949" E	
21	-		50°33'44.500" N	50°33'44.521" N	
21		-	30°17'1.994"E	30°17'3.120" E	
22	9/1.5	Culcus	50°12'47.631" N	50°12'48.601" N	
22		Culvert	29°50'16.278" E	29°50'15.890" E	
22	5/3	Culvant	50°12'41.549" N	50°12'41.876" N	
23		Culvert	29°50'11.457" E	29°50'10.381" E	
24	7/2	Culvert	50°12'53.803" N	50°12'53.443" N	
	7/3		29°52'6.471" E	29°52'6.631" E	



 $\label{eq:Figure S.1.} \textbf{Figure S.1.} \ Damage \ detection \ at \ asset \ level \ with \ LKn_H: (a) \ B1, \ -DL_H; (b) \ B2 \ , \ -DL_H; (c) \ B6, \ -DL_L; \\ (d) \ B9, \ -DL_H; \ e) \ B17, \ -DL_H$ 



 $\label{eq:Figure S.2.} \textbf{Parage detection at asset level with LKn}_{M} \textbf{: (a) B3, - DL}_{M} \textbf{; (b) B5, - DL}_{L} \textbf{; (c) B7, - DL}_{L} \textbf{; (d) B15, - DL}_{M}$ 

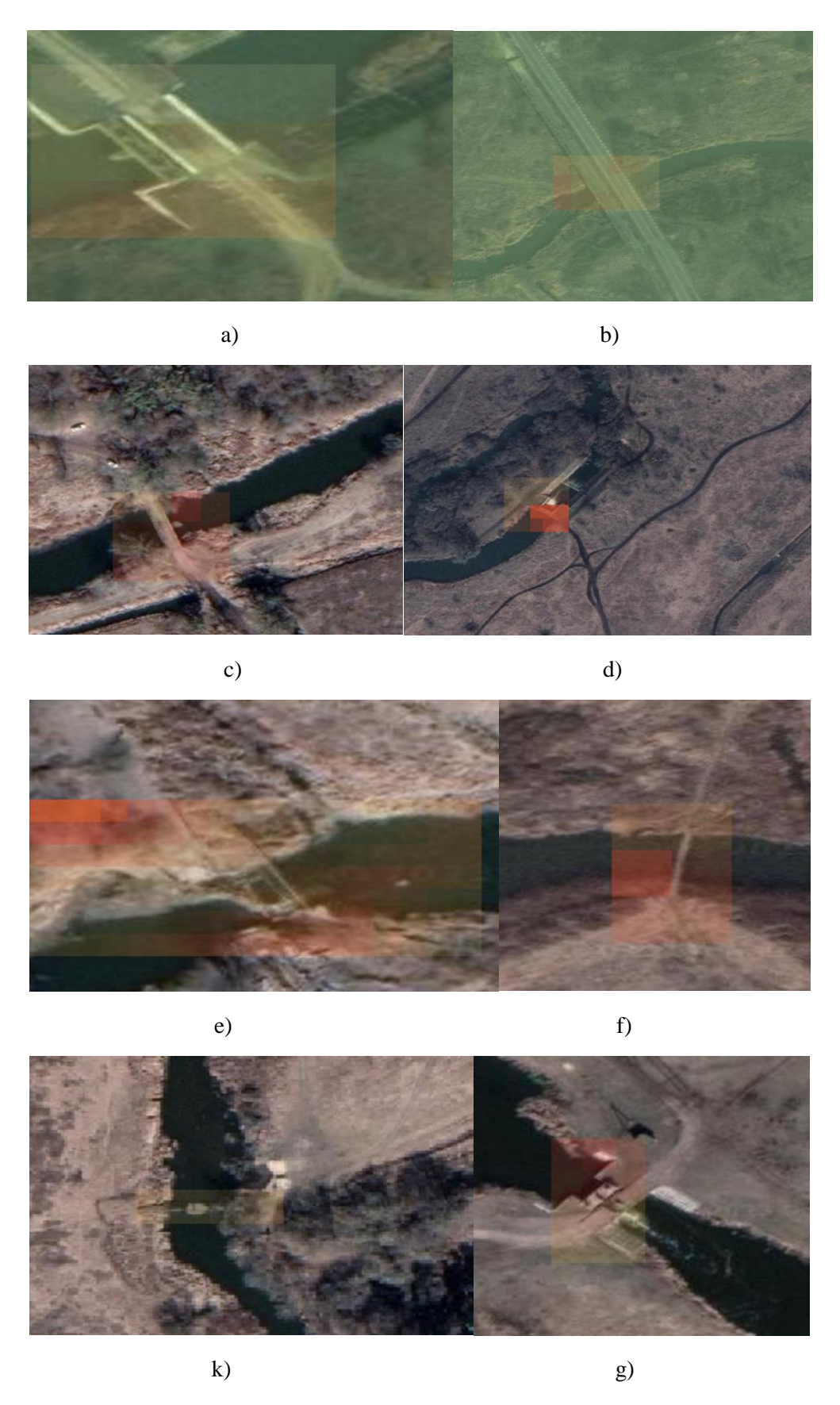


**Figure S.3.** Damage detection at asset level with  $LKn_L$ : (a) B4, -  $DL_L$ ; (b) B8, -  $DL_L$ ; (c) B10, - $DL_L$ ; (d) B11, -  $DL_L$ ; (e) B12, -  $DL_L$ ; (f) B13, -  $DL_L$ ; (k) B14, -  $DL_L$ ; (g) B16, -  $DL_L$ 

# References

- [1] De Zan F., Guarnieri A. M. TOPSAR: Terrain Observation by Progressive Scans. Geoscience and Remote Sensing, IEEE Transactions on,2006, 44(9), 2352–2360. doi:10.1109/TGRS.2006.873853
- [2] European Space Agency. Sentinel Online. (<a href="https://sentinel.esa.int/web/sentinel/home">https://sentinel.esa.int/web/sentinel/home</a>)